NASA Contractor Report 198391

Modeling of Thermal Performance of Multiphase Nuclear Fuel Cell Under Variable Gravity Conditions

S. Anghaie and Z. Ding
University of Florida
Gainesville, Florida

April 1996

Prepared for
Lewis Research Center
Under Contract NAS3–26314

National Aeronautics and
Space Administration

TABLE OF CONTENTS

ABSTRACT

A unique numerical method has been developed to model the dynamic processes of bulk evaporation and condensation processes, associated with internal heat generation and natural convection under different gravity levels. The internal energy formulation, for the bulk liquid-vapor phase change problems in an encapsulated container, was employed. The equations, governing the conservation of mass, momentum and energy for both phases involved in phase change, were solved. The thermal performance of a multiphase uranium tetrafluoride fuel element under zero gravity, micro-gravity and normal gravity conditions has been investigated. The modeling yielded results including the evolution of the bulk liquid-vapor phase change process, the evolution of the liquid-vapor interface, the formation and development of the liquid film covering the side wall surface, the temperature distribution and the convection flow field in the fuel element. The strong dependence of the thermal performance of such multiphase nuclear fuel cell on the gravity condition has been revealed. Under all three gravity conditions, 0-g, 10^{-3}-g and 1-g, the liquid film is formed and covers the entire side wall. The liquid film covering the side wall is more isothermalized at the wall surface, which can prevent the side wall from being overheated. As the gravity increases, the liquid film is thinner, the temperature gradient is larger across the liquid film and smaller across the vapor phase. This investigation provides valuable information about the thermal performance of multi-phase nuclear fuel element for the potential space and ground applications.

Nomenclature

A, C, D	constants
E	internal energy [J]
G	internal heat generation rate [kW/kg]
H	enthalpy [J]
Q	heat quantity [J] or volumetric thermal power density [MW/m^3]
T	temperature [K]
V	volume [m^3]
U	velocity [m/s]
W	work [J]
X, R	dimensionless coordinates
$c_{v,}, c_p$	specific heat at constant volume and constant pressure [J/kg/K]
e	specific internal energy [J/kg]
h	specific enthalpy [J/kg]
f	vapor phase fraction
L	length scale or the length of the container [m]
p	pressure [bar]
t	time [s]
x, r	cylindrical coordinates [m]

Nondimensional Characteristic Numbers

Gr	Grashof number

Pe	Peclet number
Pr	Prandtl number
Re	Reynolds number
Ra	Rayleigh number
St	Stefan number

Greek symbols

α	thermal diffusivity [m^2/s], or thermal diffusivity ratio
ε	phase-change temperature interval
κ	thermal conductivity [W/K/m], or its ratio
O	order of magnitude
θ	dimensionless temperature
ρ	density [kg/m^3], or its ratio
τ	dimensionless time

Subscripts

f	interface position, mixed phase
i	interface
l	liquid phase
r	characteristic scale
s, sat	saturation point
v, vap	vapor phase

Head Bar

-	nondimensional quantity

Chapter I. Introduction

The thermionic energy converter is a non-mechanical gaseous electronic device for converting heat energy directly into electric potential through thermionic electron emission. In a thermionic diode, electrons are emitted from a hot electrode, which is the emitter, and collected by a colder electrode, which is the collector, at a higher potential energy (lower electrical potential). Part of the heat removed from the emitter due to evaporating electrons is rejected to the collector by condensing electrons. The remaining heat is converted into electric power in the load as electrons return to the emitter potential. The physics governing thermionic energy conversion is well understood (Hatsopoulos and Gyftopoulos, 1973), and this energy conversion technique is attracting wide interest in its application toward a variety of power conversion systems (Lee *et al.*, 1993, Young *et al.*, 1993). In a review paper on thermionics, Rasor (1991) outlined the history, application options, and ideal performance of thermionic energy converters and described the basic plasma types associated with various modes of converter operation.

Various types of thermionic-converter systems, such as solar thermionic generators, radioisotope thermionic generators, chemical thermionic generators and nuclear reactor thermionic generators, have been or are currently being developed. The nuclear reactor thermionic generators are simply thermionic converters supplied with heat produced by nuclear fission. The fission heat is conducted from the reactor core to the emitter, and the rejected heat is conducted from the collector and carried away via a coolant. A typical schematic configuration of the thermionic fuel element (TFE) fueled with solid nuclear fuel UO_2 is shown in Fig.1.1. The nuclear fuel resides in the center of the TFE. The space between the emitter and collector is filled with an easily ionizable rarefied medium, typically cesium vapor, in order to enhance the electrical performance. A liquid metal coolant flows in the annulus channel surrounding the TFE. Recently a variety of investigations involving such a TFE have been carried out that consider the thermal

and electrical performance, system simulation and design, and application as a space power system, Lewis *et al.* (1991), McVey and Rasor (1992), Young *et al.* (1993).

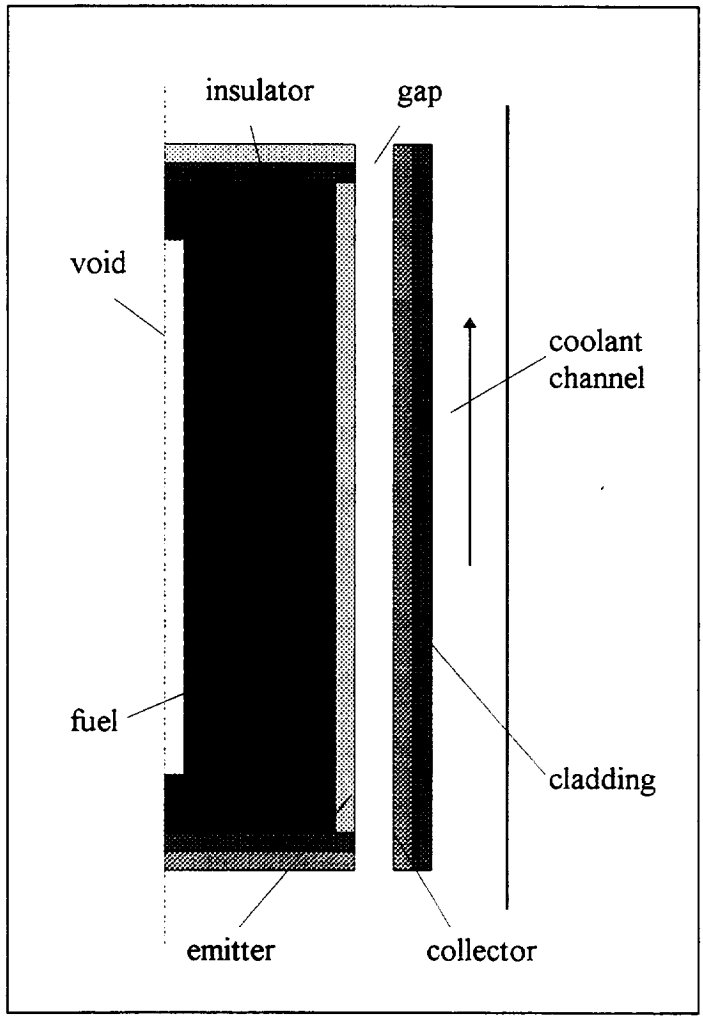

Figure 1.1 Schematic of a typical nuclear thermionic fuel element

The thermal performance of a thermionic fuel element is tightly coupled with its electrical performance. The electrical output current density is directly related to the emitter temperature,

that is, the current density increases significantly with emitter temperature, which can be illustrated by a simple example of an ideal diode thermionic converter as follows

$$J = AT_E^2 \exp[-(V + \phi_c) / kT_E]$$

where J is the current density, A and k are constants, V is the output, f_C is the collector work function, and T_E is the emitter temperature.

Consequently a nuclear fueled TFE, which can provide high temperature, is well suited for this application. The maximum operating temperature of solid nuclear fuel UO_2 could be as high as 1800 K. In order to further enhance the TFE output, a higher operating temperature is required. Such higher temperatures could be realized if liquid nuclear fuel is employed. If nuclear fuels such as UF_4 or UF_4/UO_2 in a liquid or vapor state were used, they could sustain a temperature of 2600 K or higher. The large increases in operating temperature will raise the power output significantly. The use of a multi-phase nuclear fuel reactor in conjunction with a thermionic converter provides the potential for a compact, higher power output electrical generator that is well suited for space applications.

Certain problems related to the thermal performance of TFE arise with regard to the application of multi-phase nuclear fuel reactors. These include the phase change (PC) process between the liquid and vapor, the behavior of evaporation and condensation associated with internal heating and external cooling, the location and motion of the liquid-vapor interface, the temperature distribution, the influences of gravitational fields, and so on. With such a system, particular attention must be paid to limiting the vapor pressure that is safe for the containment vessel because evaporation in a closed container will raise the vapor pressure very rapidly. A thorough investigation of these issues will be required to fully apply this concept.

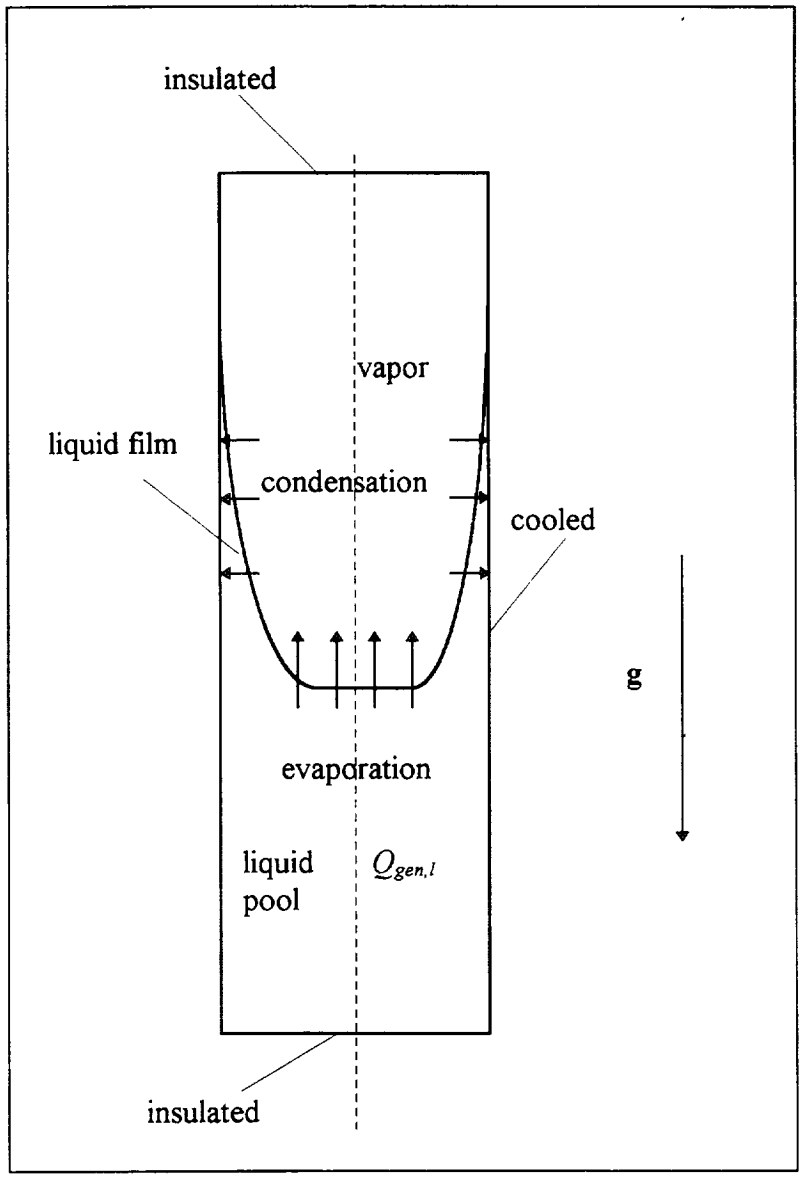

Figure 1.2 Schematic of the multi-phase nuclear fuel system

A cylindrical container filled with multi-phase nuclear fuel, such as UF_4 , is shown in Figure 1.2. The fuel experiences liquid-vapor phase change processes: evaporation and condensation. The internal heat provided by the nuclear fission reaction evaporates the liquid, while the side wall cooling tends to condense the vapor. Globally, the evaporation of liquid and condensation of vapor take place simultaneously. The evaporation and condensation processes could be driven by either pure heat conduction or by both heat conduction and convection,

depending mainly on the gravity field. Under a zero-gravity condition, buoyancy-driven convection is nonexistent. However, under micro-gravity or one-gravity fields, buoyancy-induced convection is present. The location of the liquid-vapor interface may vary depending on the mode of heat transfer, the internal heat generation intensity and spatial distribution, and the gravity field. Such an interface could be defined as a free and moving interface. To solve the phase change problem analytically or numerically, the free and moving interface is not known in advance, so that its position has to be determined as a part of the solution. Thus the solution to this heat transfer problem is quite complex.

The purpose of this work was to develop a numerical method for the computation of the bulk evaporation and condensation processes involved in a specific class of liquid-vapor phase change problems under constant volume. The phase-change behavior and thermal performance of a multiphase nuclear fuel element, operated under 0-g, micro-g and normal-g, were investigated. Certain problems are related to the application of the multiphase fuel element which include the phase-change processes between liquid and vapor, *i.e.*, the bulk evaporation and condensation, with internal heat generation, the location of the liquid-vapor interface, the temperature distribution, the influences of gravitational fields, *etc.*. The evaporation and condensation processes in the multiphase system could driven by either pure heat conduction or by both conduction and convection, depending mainly or the gravity level. Under zero-gravity condition, buoyancy driven convection does not exist. However, under micro-gravity or normal gravity fields, buoyancy induced convection is present. The location of the liquid-vapor interface may vary depending on the mode of heat transfer, the convection flow pattern, the internal heat generation rate and its spatial distribution, as well as the gravity field.

Specific issues had to be investigated for the above desired conditions. The literature appears not to contain significant work on the phase change processes between liquid and vapor, the bulk evaporation and condensation involved in the multiphase system. Very limited investigations have been conducted, *i.e.*, Shyy (1994b), Ding (1995), Ding and Anghaie (1994b, 1995a, b), in this area. To the best of the author's knowledge, no prior research has considered the general bulk condensation and evaporation processes in an enclosed container, under various gravity fields, with and without internal heat generation. Liquid-vapor phase change problems are also characterized by a large step change in the density across the phasic boundary. The singular jump of the density at the interface, other than the jump of temperature gradient which exists unavoidably for all phase change problems, brings a serious challenge to computational fluid dynamics and heat transfer.

Since the investigations for the solid-liquid phase change problems, such as melting and solidification, are numerous, some successful experiences and lessons can be drawn and applied into the study of the bulk evaporation and condensation. Appropriate modeling, such as formulation and numerical treatment have to be developed. For the solid-liquid phase change problems, the thermodynamic and transport properties between two phases vary moderately during phase change processes. The properties, however, vary significantly or dramatically during the phase change processes between liquid and vapor. Therefore, scaling and analysis of order of the magnitude have to be conducted to make simplifying assumptions that can lead to a concise and efficient solution procedure for the governing equations. Special treatment and closure relationships, such as those for vapor phase fraction, the vapor density, the saturation pressure and temperature, had to be applied and implemented into the computation.

Like all phase change processes, evaporation and condensation are also inevitably subject to the effect of convection induced by either buoyancy or surface tension variations. The existence of the convection can substantially affect the flow field, the temperature field, and subsequently the performance of the phase change process. The effect of the convection on the evaporation and condensation processes are to be investigated. For the conventional solid-liquid phase change problems, heat is usually provided externally from the boundary to the system. For the nuclear system, heat is generated internally via nuclear fission reaction. The problems of phase change induced by internal heating are different from those induced by external heating and need to be investigated too. The internal heating, like the external heating, results in the temperature and density distribution, and consequently causes the buoyancy effect. Such natural convection induced by internal heating is defined as internal natural convection, to be distinguished with the classical natural convection caused by external heating/cooling. This internal natural convection has drawn the attention of a few investigations, *i.e.*, Acharya and Goldstein (1985), Lee and Goldstain (1988), Ding(1995). The behavior of the internal natural convection and its influence on the phase change processes, in particular on the bulk evaporation and condensation processes, were investigated in these studies.

Previous investigations of phase-change problems are numerous but limited to a few types. Those activities, which can be traced back as early as Clausius, Clapeyron, Stefen, Nusselt, *etc.*, have been conducted both experimentally, analytically and are currently being attempted using numerical simulations and approximation methods. In their annual review papers, Eckter *et al.*, (1990, 1991 and 1992), suggested that most of these current works have focused on: melting and solidification, pool and flow boiling, film and droplet evaporation, filmwise and dropwise

condensation, with applications in thermal energy storage, solidification of alloys and metals, casting processes, crystal growth, heat pipes, heat pumps, boilers, heat exchangers, and nuclear or chemical reactors. The major characteristics and classification of a group of phase change problems, and the current research activities and status are summarized in Table 1.1.

Table 1.1 Brief summary of major characteristics of phase change problems

Moving Boundary - Phase Change Problems						
PC Between	Solid - Liquid		Liquid - Vapor			
Process	Melting and solidification		flow or pool boiling	film or drop conden-sation	**bulk evaporation and condensation**	
Heating /Cooling	externally from the system boundary		externally from boundary		**externally or internally heating**	
Thermo-physical properties	constant or change moderately		**change significantly or drastically**			
Conduction and/or convection	conduction only	conduction and convection	conduction and convection		**conduction only**	**conduction and convection**
Solution Approach	analytical numerical empirical	numerical empirical	experimental numerical analytical		**numerical**	
Research Status	numerous investigations		numerous investigations		very few found, **being conducted**	

Early analytic work on phase change between solid and liquid included studies by Lame and Clapeyron (1831) and Stefan (1891). The fundamental features of this type of problem and some basic analytical solution methods were discussed by Ozisik (1980), Crank (1984) and Yao *et al.* (1989). Crank (1984) presented a broad but reasonably detailed account of the mathematical solution, both analytical and numerical, of these problems. Due to the existence of the interface, difficulties were encountered in solving these problems to the extent that only a handful of very simple cases can be theoretically analyzed.

Since the 1970's, greater attention and interest have been paid to purely numerical analysis and simulations, which is reflected in the large number of publications covering these topics, *i.e.*, Crank (1984), Voller *et al.* (1987, 1991), Yao *et al.* (1989), Brice (1986), Brown (1988), Gau and Viskanta (1986), Nadarajah and Narayanan (1990), Shyy *et al.* (1990, 1991, 1992a, b, 1994a, 1995) and Shyy (1994a, b, 1995). In his book, Shyy (1994a) summarized a substantial portion of his research activities, and presented the various computational elements important for the prediction of complex fluid flows and interfacial transport.

Recent years have also witnessed a growing interest in other forms of phase change processes, such as evaporation and condensation. Carey (1992) systematically summarized the state of the art in boiling and/or condensation phenomena. That book focuses on some fundamental elements and the basic physical mechanism of condensation and vaporization processes and provides a broad review of the research activities in these areas. Among the investigations on condensation and evaporation, those on film condensation are well developed, particularly on laminar film condensation, due to its simplicity. The development of the current theory and the prediction of heat transfer rates associated with film condensation have its origin in the analyses presented by

Nusselt (1916). Subsequently, many modifications of this analysis have appeared, each one further relaxing the restrictive assumptions of the Nusselt analysis. Considerations have been given to gravity-flow condensation, pure forced convection condensation in the presence of a body force, such as in Sparrow *et al.* (1967) and Rohsenow (1973). Recently some studies on general film condensation transients and the interfacial condensation model have been conducted by Filk and Tien (1989) and Gerner and Tien (1989). With the development of computational fluid dynamics and numerical heat transfer, more and more attempts have been made to model and simulate condensation phenomena, for example, Jones and Renz (1974), Cossmann, Odenthal and Renz (1982), and Gaultier *et al.* (1993). However, most of these activities, either analytical or numerical, have focused on flow condensation problems with open plates, channels or open containers where the vapor pressure, saturation temperature and latent heat are maintained constant. These problems, where forced convection plays a dominant role, are usually parabolic type problems, and consequently are much simpler than those in the present study in which the saturation temperature, pressure and latent heat continuously change. A few computational simulations of evaporation in containers have been carried out recently. Jang *et al.* (1990) modeled a heat pipe start-up from the frozen state by using one dimensional equations for different phases. Shyy (1994b) developed a computational method for predicting the two-phase transient flow and heat transfer characteristics within a constant pressure reservoir of a capillary-pumped-loop and investigated the phase change of liquid and vapor, under various conditions. Ding and Anghaie (1994a, 1995a, b), Anghaie and Ding (1995), Ding (1995) developed a modeling procedure for the bulk evaporation and condensation and applied it into the investigation of multi-phase nuclear fuel systems.

Considerable attention has been given to the study of natural convection of single phase fluid in enclosures. The temperature gradients across the system are supplied externally to induce the density gradients and consequently the buoyancy driven flows. A great deal of research, both numerical and experimental, on various types of convective heat transfer problems has been conducted, *i.e.*, Ostrach (1982, 1983, 1988), Gebhart *et al.* (1988), de Vahl Davis (1983), Hortmann *et al.* (1990), Shyy *et al.* (1992b), Shyy (1994a), Bejan (1984), Carpenter *et al.* (1989), Ramaswamy *et al.* (1992), Bergman *et al.* (1981), *etc.*. Ostrach (1982, 1983, 1988), Gebhart *et al.* (1988) and Bejan (1984) reviewed and summarized those activities and achievements. Among the large number of the natural convection problems, the buoyancy-driven flow in a square cavity with vertical side walls heated differentially, so called a bench mark problem for natural convection, is a suitable vehicle for testing and validating computer codes. Accurate benchmark solutions have been published by De Vahl Davis (1983) and by Hortmann *et al.* (1990) and are available for comparison with the present computations.

Natural convection induced by external heating is of importance in many applications. Natural convection in an enclosure in which the internal heat generation is present is also of prime importance in certain technological applications. Examples are post-accident heat removal in nuclear reactors and some other geophysical or astrophysical problems. Natural convection induced simultaneously by external heating and internal energy sources, however, in contrast to the extensive investigations on the conventional external heating convection problems, has received very limited attention, such as Archarya and Goldstein (1985), Lee and Goldstein (1988), Fusegi *et al.* (1992), Ding (1995). The presence of internal heat generation provides an additional

dynamic in overall convective flow systems and offers a complicated yet challenging aspect of the convection under consideration.

With no exception, convection induced by either buoyancy or surface tension variations will also be involved in evaporation and condensation like all phase change problems. The involvement of the convection can substantially affect the phase change process. Numerous investigations on the solid-liquid phase change problems with convection can be found in Ostrach (1983), Crank (1984), Brice (1986), Brown (1988), Gau and Viskanta (1986), Nadarajah and Narayanan (1990), Shyy *et al.* (1990, 1991, 1992a, b, 1994a, 1995) and Shyy (1994a, b, 1995), *etc.*.

Chapter II. Thermal Performance of Multiphase UF_4 Fuel Element at Zero Gravity

2.1 The Internal Energy Formulation

The first law of thermodynamics, for any closed thermodynamic system, is

$$\delta Q = dE + \delta W = dH - (pdV + Vdp) + \delta W \tag{2.1}$$

where E is the internal energy, H is enthalpy, Q is the heat input, W is the work output, p and V are the pressure and volume of the system, respectively. For the phase change process involved in the rigid and enclosed container with constant volume, there is no mechanical work. Therefore the first law for this closed and rigid system reduces to

$$\delta Q = dE = dH - Vdp \tag{2.2}$$

which indicates that the heat exchange between the system and the ambient causes the internal energy, the enthalpy and pressure of the system to change. Therefore the released or absorbed latent heat associated with the phase change induces the changes of internal energy, enthalpy and pressure. The quantity of the heat exchange is equal to the internal energy change, but not equal to the enthalpy change. The conventional enthalpy formulation of the energy equation, commonly used for the phase change between solid and liquid, should include a transient pressure term for this phase change between liquid and vapor. The weak form of the energy equation based on enthalpy formulation is

$$\rho \frac{Dh}{Dt} = \frac{Dp}{Dt} + \nabla \cdot (\kappa \nabla T) \tag{2.3}$$

This formulation including the transient pressure term introduces additional complexity and does not seem to be the best choice for this problem. A more attractive alternative, the internal energy based formulation for the energy equation which does not include the pressure term, is proposed and developed in this work. Similar to the enthalpy formulation used for melting

and solidification problems, the internal energy formulation does not require to explicitly track the interface position. The weak form of the energy equation with internal energy as the primary variable can be expressed as follows:

$$\rho \frac{De}{Dt} = \nabla \cdot (\kappa \nabla T) \tag{2.4}$$

where the internal energy e may be expressed, in the form of a summation of sensible heat and latent heat, for the liquid, vapor and mixed phases as:

$$\begin{aligned} e &= c_{v,l} T && f = 0 \\ e &= c_{v,l} T_{sat} + f \Delta e && 0 < f < \\ e &= c_{v,l} T_{sat} + \Delta e + c_{v,v} (T - T_{sat}) && f = 1 \end{aligned} \tag{2.5}$$

where T_{sat} is the saturation temperature, Δe is the internal energy difference between saturated vapor and saturated liquid (latent heat), and the constant volume specific heat c_v's are functions of temperature provided by Reynolds (1979). The vapor phase fraction f is zero in the region filled with liquid phase and unity in the region occupied by vapor phase. The vapor phase fraction lies between zero and unity when the control volume is undergoing phase change.

Substituting Eq.(5) into the governing Eq.(4) yields

$$\begin{aligned} \rho_l \frac{D}{Dt}(c_{v,l} T) &= \nabla \cdot (\kappa_l \nabla T) && f = 0 \\ \rho_f \frac{D}{Dt}(c_{v,f} T) &= \nabla \cdot (\kappa_f \nabla T) - \rho_f \Delta e \frac{Df}{Dt} && 0 < f < 1 \\ \rho_v \frac{D}{Dt}(c_{v,v} T) &= \nabla \cdot (\kappa_v \nabla T) && f = 1 \end{aligned} \tag{2.6}$$

where the latent heat now appears as a source term. The form of this internal energy based equation is identical to that of the enthalpy based equation, except the pressure term appearing in

the later one. Just like the enthalpy formulation, this internal energy formulation is also a single region formulation, where one set of governing equations can describe both phases. A major advantage of the internal energy formulation is that it is not necessary to split the domain into separate subdomains consisting of different phases. A fixed grid can be employed to facilitate the computations.

Both enthalpy formulation and internal energy formulation are implemented and examined. The vapor phase fraction, f, may be defined in two different ways, which can lead to different update methods.

Some additional closure relations are required for the multiphase condition in the container. Property variations are based on a simplified searching routine. The different phases are differentiated based on the local temperature or internal energy at each nodal point, within the frame work of the temperature based or internal energy based update method. Using temperature based update, the liquid or the vapor phase is identified by the local temperature, wherever the temperature at any point is lower than the saturated liquid temperature or higher than the saturated vapor temperature, that point is located in the liquid or vapor region, respectively. Similarly, if the internal energy based update is used, the liquid or the vapor phase is identified by the local internal energy. Either case allows the vapor phase fraction in a computational cell to be calculated. Using the Clausius-Clapeyron equation, the saturation temperature as a function of the system pressure is calculated:

$$T_{sat} = \frac{C}{D - \ln p_{sat}} \tag{2.7}$$

where C and D are constants.

The saturation pressure, or the vapor pressure, can be obtained from the approximate equation of state for an ideal gas, and the mass conservation in which the bulk vapor density and temperature are used:

$$p_{sat} = p_{vap} = \frac{m_v}{V_{vap}} R T_{b,vap}, \qquad m_{total} = m_V + m_l = Constant \tag{2.8}$$

where R is the gas constant for vapor phase. Eqs.(2.7) and (2.8), have been proposed and used as the basis for the model developed by the authors, Ding and Anghaie (1994a, b, 1995a, b, c), Anghaie and Ding (1995).

2.2 The Governing Equations

Based on the modeling procedure developed in the previous section, the bulk evaporation and condensation processes with internal heat generation under zero gravity condition were studied. The system, at a certain steady state, filled with liquid and vapor is shown as Fig. 1.2. Since the system is designed to operate under 0-g of the space environment, there is no buoyant effect and natural convection. Initially, the vapor and liquid are kept saturated at a certain pressure and uniform temperature. The top wall and bottom wall are insulated. The side wall is cooled with a lower constant temperature or constant heat flux. The internally generated heat evaporates the liquid, while the cold side wall removes the heat from the liquid-phase and condenses the vapor-phase. For this system with such an orientation and operating under 0-g, there is no bubble or droplet generation on the wall surface. The temperature along the liquid-vapor interface does not change significantly according to the Gibs-Thomson relation (see Shyy 1994a), because the curvature of the interface is moderate. The liquid-vapor interface can be reasonably assumed as isothermal, consequently the thermal capillary effect can be neglected.

Hence the phase-change process is entirely driven by the internal heat generation and heat conduction. The rate of evaporation or condensation is determined by the local temperature distribution. The time dependent and non-uniform internal heat generation results in a transient temperature distribution and causes the motion and deformation of the interface.

The internal energy formulation of the energy equation for this phase-change process with the constraint of constant volume is used. The weak form of the energy equation for conduction is

$$\rho\frac{\partial e}{\partial t} = \nabla\cdot(\kappa\nabla T) + Q_{gen} \tag{2.9}$$

The source term Q_{gen} is the internal heat generation rate, representing the thermal power density released via nuclear fission reaction, which varies with time and space according to the following relation:

$$Q_{gen} = \rho G(t)\cdot\sin(\frac{\pi x}{L}) \tag{2.10}$$

where G*(t)* is a time dependent volumetric heat generation rate, ρ is the local phase density, L is the length of the container. Some additional closure relations, the same as Eqs.(2.7) and (2.8) are required for the multiphase condition in the container.

The governing equation (2.9) is normalized and expressed for different phases as:

$$\begin{aligned}
&\overline{\rho}_l\frac{\partial\theta}{\partial\tau} = \overline{\kappa}_l\nabla^2\theta + \overline{Q}_{gen,l} && f=0\\
&\overline{\rho}_f\frac{\partial\theta}{\partial\tau} = \overline{\kappa}_f\nabla^2\theta + \overline{Q}_{gen,f} - \overline{\rho}_f\frac{1}{St}\frac{\partial f}{\partial\tau} && 0<f<1\\
&\overline{\rho}_v\frac{\partial\theta}{\partial\tau} = \nabla^2\theta + \overline{Q}_{gen,v} && f=1
\end{aligned} \tag{2.11}$$

where S_t is the Stefan number defined as $c_v T_{s,0}/\Delta\varepsilon$. The nondimensional heat generation rate is

$$\overline{Q}_{gen,i} = \overline{\rho}_i \overline{G}(\tau)\sin(\pi X) \tag{2.12}$$

where $\overline{G}(\tau) = G(t)(tr/c_v T_{s0})$. The initial saturation temperature $T_{s,0}$ and the length of the container are chosen as the characteristic temperature scale and length scale, respectively. The characteristic time scale is $tr = L^2/\alpha_v$ which is the thermal diffusion time scale in the vapor phase. The E-based update method discussed previously is used for the iterative update of the vapor fraction.

2.3 Thermophysical Properties of Uranium Tetrafluoride

The nuclear fuel uranium tetrafluoride, UF_4 , is used to provide heat to the system. The thermophysical properties of its liquid and vapor at a reference state of T_0=2000K and, P_0=1Mpa (10 atm), are given in Table 2.1 according to Watanabe and Anghaie (1993) and Anghaie (1992).

Table 2.1 Thermophysical Properties of UF_4 Liquid and Vapor at T_0=2000K, P_0=1Mpa.

Properties	c_p	c_v	R	ρ	κ	μ	Pr
Unit	J/kg/K	J/kg/K	J/kg/K	kg/m^3	W/m/K	kg/m/s	
Vapor	345	320	25	20	0.06	8.5×10^{-5}	0.53
Liquid	480	480		6000	0.5	5.2×10^{-4}	0.89

where **R** is the gas constant. Some assumptions and simplifications have to be made based on the order and scaling analysis as discussed before. All the properties, except the vapor density, are assumed constant. The vapor phase is assumed to be the an ideal gas. The vapor density is obtained from the equation of state for a perfect gas. In the governing equation (2.11), the thermal conductivity ratio of liquid to vapor is $\overline{\kappa} = \dfrac{\kappa_l}{\kappa_v} = 8.3$, and the density ratios of liquid to vapor at the referential state is $\overline{\rho}_0 = \dfrac{\rho_l}{\rho_{v,0}} = 3\times10^2$, where the subscript 0 denotes a referential state. The Stefan number, $St = c_v T_0/\Delta e$, is 0.67 where Δe is the latent heat which is involved with

phase change. The characteristic time scale $tr=L^2/\alpha_v$ =280 seconds. The dimensionless time dependent parameter for heat generation rate expressed in Eq.(2.12) is given by

$$\begin{aligned} \overline{G}(\tau) &= 4\tau & 0 \le \tau \le 1.5 \\ \overline{G}(\tau) &= 4 \times 1.5 = 6 & > 1.5 \end{aligned} \qquad (2.13)$$

Thus the real parameter B(t) is

$$\begin{aligned} G(t) &= 33 \times t & 0 \le t \le 420 \\ G(t) &= 33 \times 420 = 13.86 \quad (kW/kg) & t > 420 \quad (s) \end{aligned} \qquad (2.14)$$

Correspondingly, the maximum thermal power density in the liquid phase, at the final steady state or the full power state when t > 420 s, is $Q_{gen,l}|_{\max} = \rho_l G(t > 420s) = 83(MW/m^3)$. The average power density, including the spatial distribution and vapor phase, for the entire fuel cell is

$$Q_{gen,}|_{average} = 0.5 \times Q_{gen,l}|_{\max} \int_0^L \sin(\pi x)dx = 0.5 \times Q_{gen,l}|_{\max} \times \frac{2}{\pi} = 26.5(MW/m^3) \qquad (2.15)$$

2.4 Results and Discussion

The second order central difference scheme for the spatial differential terms and the fully implicit marching scheme for temporal term are adopted to solve Eq. (2.11). A uniform mesh of 101x41 grids covers the liquid phase and vapor phase within the container, and another non uniform mesh with 101x5 grids covers the side wall region. The outer surface of the side wall is cooled by a constant heat flux.

Because of symmetry, only the right half of the container is considered. Initially, the lower half of the container is filled with liquid and the upper half is occupied by vapor. The aspect ratio

of the container is 2.5. The initial saturated vapor and liquid temperature is 2000K. At t=0, the side wall is cooled at a constant heat flux, and the internal heat starts to be generated.

The evolution of the evaporation/condensation process is shown in Fig.2.1. Using the phase identifier which is the local vapor phase fraction, the distribution of the liquid and vapor phases and the position of the interface are determined. The topology of the liquid-vapor interface and the temperature distribution at various time instants are displayed in the top and bottom rows of Fig.2.1, respectively. The internal heat generation evaporates the liquid, while the side wall cooling tends to condense the vapor. Globally, the evaporation of liquid and condensation of vapor take place simultaneously, as shown schematically in Fig.1.2. The local phase-change process, whether evaporation or condensation, is dominated by the local internal heating or by the wall cooling effect, since the internal heat generation is a spatial function. The evaporation is dominant near the central axial position where the heat generation intensity is higher and evaporates more liquid. The condensation caused by the side wall cooling is dominant near the axial end and side wall where the heat generation density is lower. The simultaneous evaporation and condensation cause the motion and deformation of the interface. Because of the time dependent heat generation, the local evaporation and condensation, the motion and deformation of the interface continue.

As the process evolves, certain amount of liquid is evaporated into vapor due to the internal heat generation which is increasing at the early period, as Eq.(2.14) indicates. Meanwhile, some amount of vapor near the side wall is condensed into liquid due to the cooling of the side wall. During earlier periods, a short piece of liquid film is formed along the side wall owing to the condensation, and the liquid-vapor interface becomes concave because of the evaporation. With

time increasing, the interface keeps moving and deforming. The liquid film grows longer and thicker, and the position of the interface at the centerline of the container descends lower and lower. When t = 112 s, or $\tau = 0.4$, the liquid film grows up to the top end and covers the entire side wall. The liquid phase which is initially filled in the lower part of the container now forms a long film covering and residing along the entire side wall. At t = 392 s ($\tau=1.4$), the interface at the low central side descends quite close to the bottom end. After t = 420 s ($\tau=1.5$), the internal heat generation rate is a constant as indicated by Eq. (2.14) and the cooling heat flux at the side wall is still kept constant, the system reaches a steady state and the interface no longer moves. The topology of the interface strongly depends on the temperature distribution and the internal heat generation rate distribution which now is independent of time but only a spatial function. The shape of the interface follows approximately the heat generation distribution in a form of chopped sine function.

During the transient process, the temperature distribution varies with the time. The temperature contours for the entire system become denser and denser gradually, since the internal heat generation is increasing. After the steady state is reached, the axial and radial temperature distributions follow approximately the forms of chopped sine and cosine function, respectively, due to the nature of the heat generation distribution as shown in Eq. (2.12). There is a temperature gradient jump at the interface due to the release or absorption of the latent heat associated with the phase change. The discontinuity of the temperature gradient can be observed more clearly in a three dimensional temperature distribution displayed in Fig.2.2. There is an obvious fold on the temperature surf where the liquid-vapor interface is located exactly. The maximum temperature near the central axial position in the vapor region is about 4000K. The

axial temperature profile on the side wall is also in an approximate form of chopped sine function, but much flatter than that in the vapor region. The liquid is a much better conductor than the vapor, the liquid film covering the side wall is more isothermalized. This isothermalization effect is expected to satisfy the design feature of the multiphase fuel cell to be possibly applied in space. The formation of the liquid film and its full coverage on the side wall can prevent the side wall from being overheated, which is also the expectation for the application of such multiphase fuel cell.

The transient characteristic of this system can also be seen from the variation of the saturation temperature with the time shown in Fig. 2.3. The saturation temperature decreases a little bit in the early time period when the internal heating is very weak, the side wall cooling effect and condensation are dominant. As the internal heating rate increases, the evaporation becomes dominant and the saturation temperature rises. After t = 420 s ($\tau = 1.5$), as the system gradually reaches the steady state, the evaporation and condensation are balanced and the saturation temperature reaches a constant about 3000K.

The operation in the zero gravity environment is ideal and unrealistic. The study conducted in this chapter, however, provides a basis for further discovering and exploring the fundamental performances and features of such multiphase and internally heated system. The present results will be used as reference to be compared with the performances and features of this system operated under micro-gravity conditions, which will be presented in the next chapter.

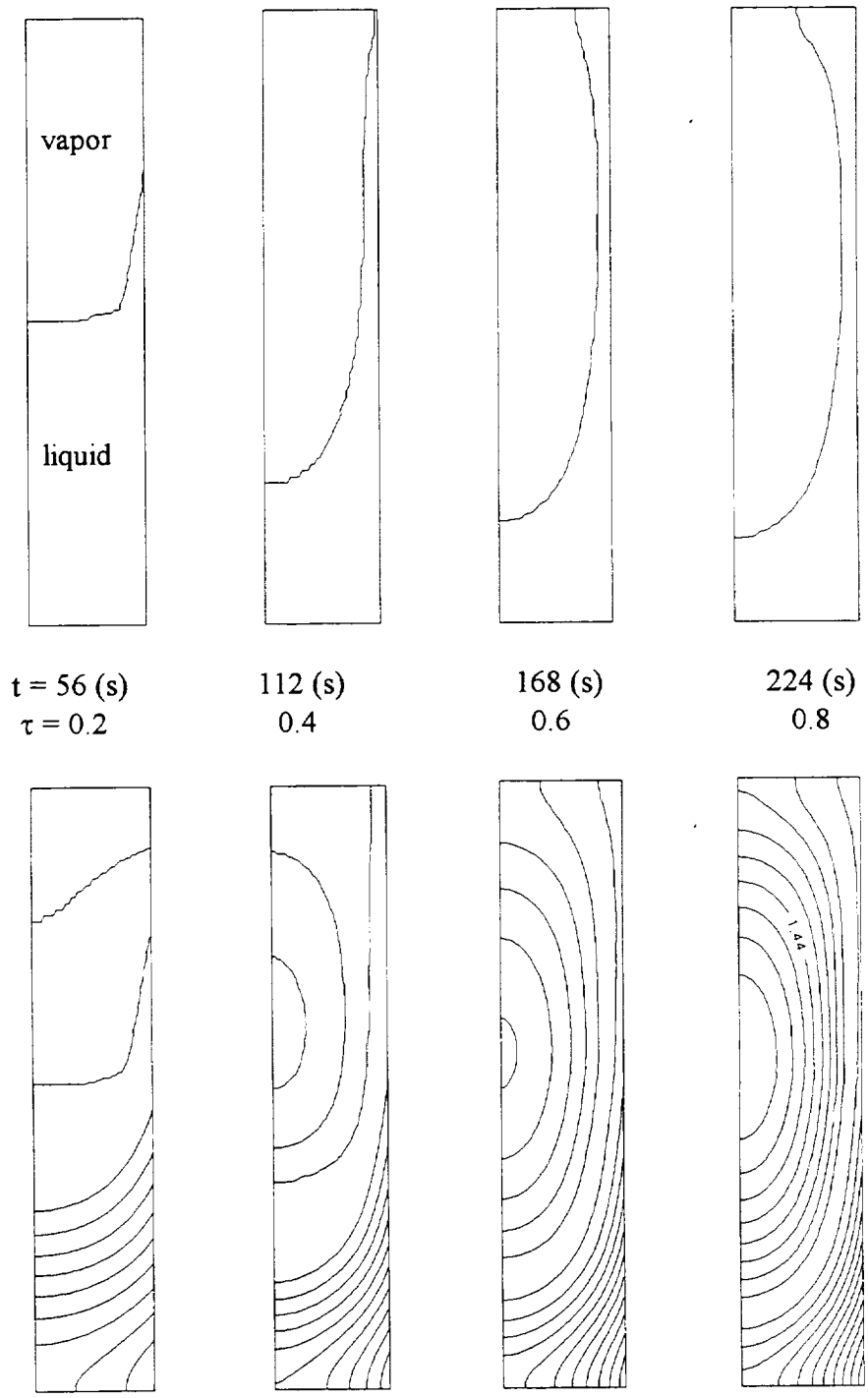

Figure 2.1 The evolution of interface and isotherm (0-g)

(top row: interface topology; bottom row: isotherm with $\Delta\theta = 0.03$, ΔT=60K, the real temperature is $T=\theta x T_0=\theta x 2000K$)

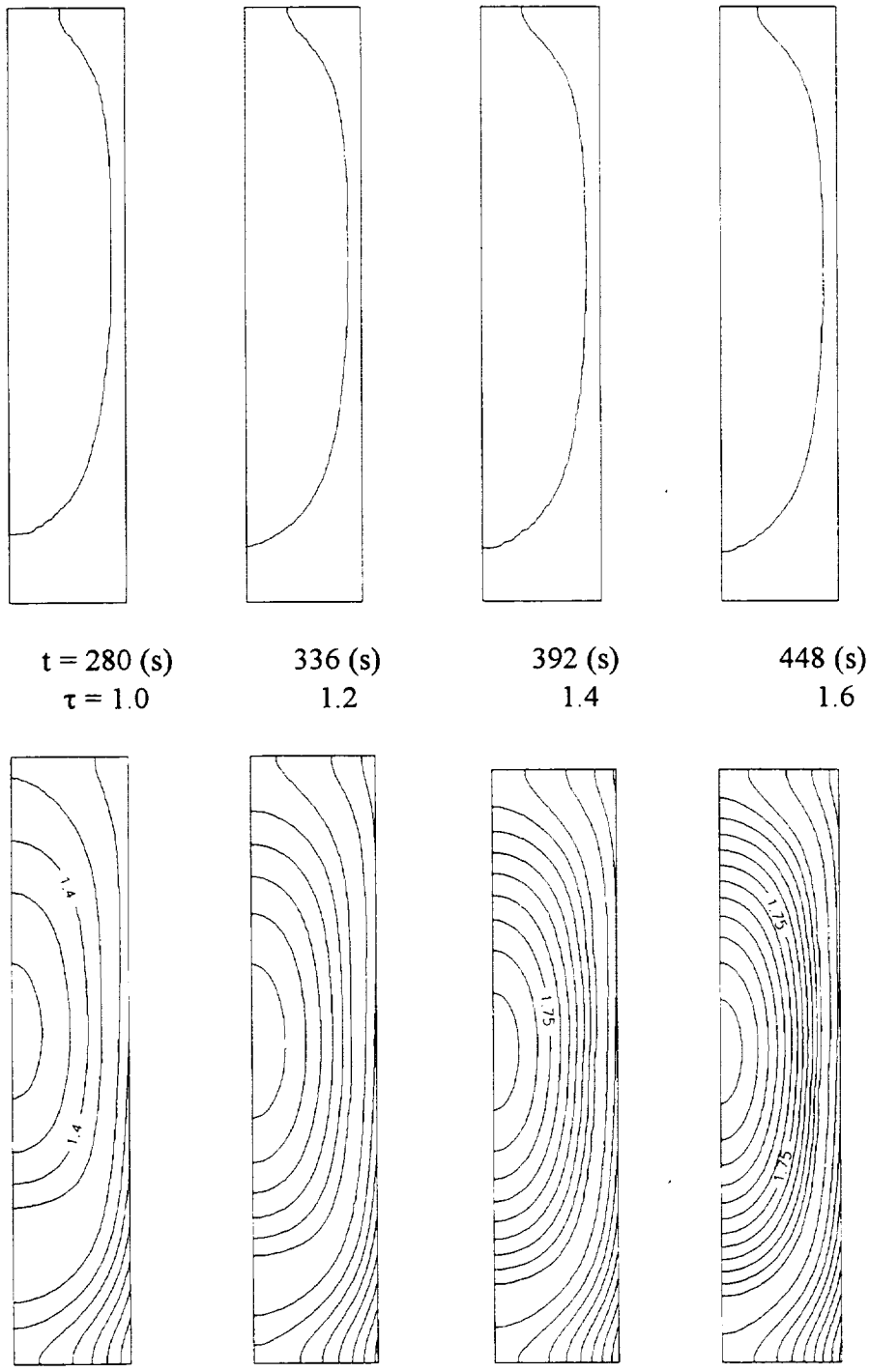

Figure 2.1 (contined) The evolution of interface and isotherm (0-g)

(top row: interface topology; bottom row: isotherm with $\Delta\theta = 0.05$, ΔT=100K, the real temperature is $T=\theta x T_0=\theta x 2000K$)

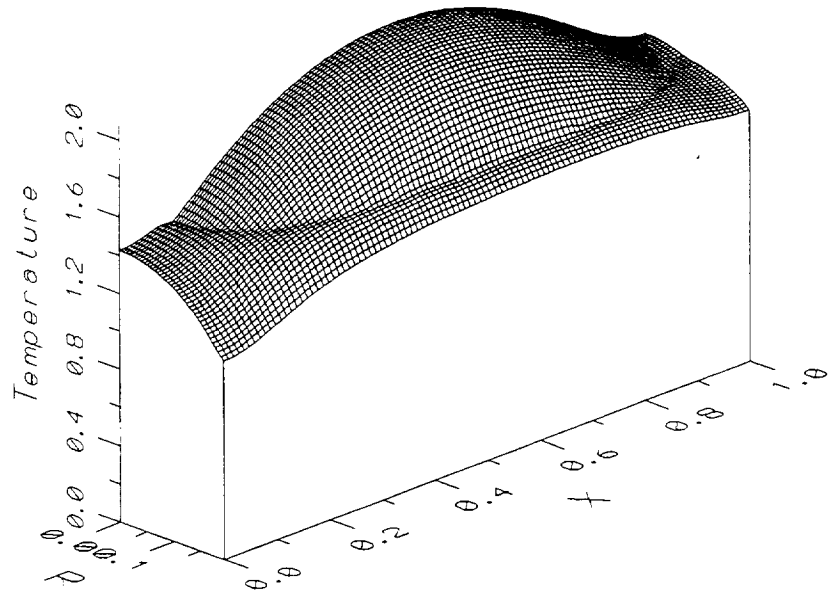

Figure 2.2 Temperature surf of the system at steady state (0-g)
(r = RxL = 0 ~ 0.01 m, x=XxL = 0 ~ 0.05 m, the real temperature is $T=\theta x T_0=0 \sim 4000K$)

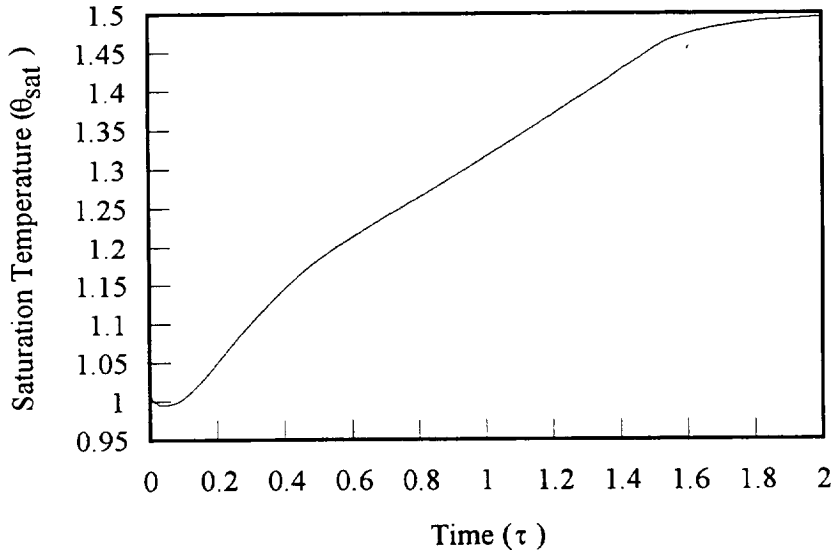

Figure 2.3 Variation of saturation temperature (0-g)
(the real time period: 0 ~ 2800 s ; the real temperature : $T=\theta x T_0=\theta x 2000K$)

Chapter III. Modeling of Thermal Performance of Multiphase UF_4 Fuel Element at Micro-Gravity and Normal Gravity

3.1 Brief Preview

So far, only conduction dominated effects under limited conditions have been taken into account for the bulk evaporation and condensation processes. Like all phase change processes, evaporation and condensation are also inevitably subject to the influences of convection induced by either buoyancy or surface tension variations. The existence of convection can substantially affect the flow field, the temperature field, and subsequently the performance of the phase change process.

Numerous investigations on the phase change with convection have been conducted, which can be found in Ostrach (1983), Crank (1984), Brice (1986), Brown (1988), Gau and Viskanta (1986), Nadarajah and Narayanan (1990), Shyy *et al.* (1990, 1991, 1992a, b, 1994a, 1995) and Shyy (1994a, b, 1995), *etc.*

In this chapter, the modeling of the bulk evaporation and condensation processes, associated with internal heat generation and under various gravity levels, is presented. The system to be modeled is Fig.1.2. The nuclear fuel uranium tetrafluoride, UF_4, is used to provide heat to the system. The top wall and bottom wall are insulated. The side wall is cooled externally by a constant outward heat flux which removes heat from the system and tends to condense the vapor phase. The internal heat generation provides heat to evaporate the liquid phase. Since the system is to be operated under different gravity conditions, there is convection, both in the liquid and vapor phases, induced by buoyancy force due to the density variation. The temperature along the liquid-vapor interface will not change significantly according the Gibs-Thomson relation (see Shyy

1994a, 1995), because the curvature of the interface is moderate. The liquid-vapor interface can be reasonably assumed as isothermal, thus the thermal capillary effect can be neglected. The phase change processes are controlled by conduction and convection. The performances of the phase change can be quite different at various gravity condition, as we can expect. The flow field, the temperature distribution and the motion of the interface are strongly dependent on the g-levels, as will be demonstrated later.

3.2 The Governing Equations

The governing equations describing the phase change process with the natural convection in both phases, in the cylindrical coordinate system, in original dimensional form are

$$\frac{\partial \rho_i}{\partial t} + \nabla \bullet (\rho_i \vec{V}) = 0 \tag{3.1}$$

$$\frac{\partial \rho_i u}{\partial t} + \nabla \bullet (\rho_i \vec{V} u) = -\frac{\partial p}{\partial x} + \nabla \bullet (\mu_i \nabla u) - \rho_i g \tag{3.2}$$

$$\frac{\partial \rho_i v}{\partial t} + \nabla \bullet (\rho_i \vec{V} v) = -\frac{\partial p}{\partial r} + \nabla \bullet (\mu_i \nabla v) \tag{3.3}$$

$$\frac{\partial \rho_i c_v T}{\partial t} + \nabla \bullet (\rho_i \vec{V} c_v T) = \kappa_i \nabla^2 T + \rho_i G(t) \sin(\pi \frac{x}{L}) - \Delta e \frac{\partial (\rho_i f)}{\partial t} - \Delta e \nabla \bullet (\rho_i \vec{V} f) \tag{3.4}$$

where the subscript $i=l,\ v$ denotes the liquid and vapor phases respectively, $\rho_{v,0}$ is the referential vapor density, $G(t)$ is the volumetric internal heat generation rate. The thermal expansion coefficient, β, is introduced into the u-momentum equation to expand the buoyancy term, according to the Boussinesq approximation

$$\rho_i = \rho_{i,0}[1 - \beta_i (T - T_0)] \tag{3.5}$$

Therefore we have

$$\begin{aligned} & -\rho_i g \\ & = g\rho_{i,0}[\beta_i(T-T_0)-1] \\ & = g\rho_{i,0}\beta_i T_0(\theta-1)-g\rho_{i,0} \end{aligned} \tag{3.6}$$

where the first term represents just the conventional buoyancy effect caused by the density variation in a single phase, while the second one is the global body force, or the bulk gravity force acted on the fluid at referential state.

Equations (3.1) ~ (3.4) can be normalized as

$$\frac{\partial \overline{\rho}_i}{\partial \tau} + \nabla \bullet (\overline{\rho}_i \vec{\overline{V}}) = 0 \tag{3.7}$$

$$\frac{\partial \overline{\rho}_i U}{\partial \tau} + \nabla \bullet (\overline{\rho}_i \vec{\overline{V}} U) = -\frac{\partial \overline{P}}{\partial X} + \mathrm{Pr}_v \nabla \bullet (\overline{\mu}_i \nabla U) + \overline{g} Ra_v \mathrm{Pr}_v \overline{\rho}_{i,0}[\overline{\beta}_i(\theta-1) - \frac{1}{\beta_v T_0}] \tag{3.8}$$

$$\frac{\partial \overline{\rho}_i V}{\partial \tau} + \nabla \bullet (\overline{\rho}_i \vec{\overline{V}} V) = -\frac{\partial \overline{P}}{\partial R} + \mathrm{Pr}_v \nabla \bullet (\overline{\mu}_i V) \tag{3.9}$$

$$\frac{\partial \overline{\rho}_i \theta}{\partial \tau} + \nabla \bullet (\overline{\rho}_i \vec{\overline{V}} \theta) = \overline{\kappa}_i \nabla^2 \theta + \overline{\rho}_i \overline{G}(\tau)\sin(\pi X) - \frac{1}{St}\frac{\partial(\overline{\rho}_i f)}{\partial \tau} - \frac{1}{St}\nabla \bullet (\overline{\rho}_i \vec{\overline{V}} f) \tag{3.10}$$

where $\overline{g}$ is the gravity factor representing the gravity level. The Rayleigh number, based on the ground gravity level and vapor properties, is defined

$$Ra_v = \frac{g\beta_v T_0 L^3}{\alpha_{v,0}\nu_{v,0}} \tag{3.11}$$

The Prandtl number for vapor phase is

$$\mathrm{Pr}_v = \frac{\nu_{v,0}}{\alpha_{v,0}} \tag{3.12}$$

The nondimensional internal heat generation rate is

$$\overline{G}(\tau) = \frac{G(t)}{c_v T_{s,0} / tr} \tag{3.13}$$

where $tr=L^2/\alpha_{v,0}$ is the thermal diffusion time scale.

The liquid Rayleigh number and Prandtl number are also implicitly included in the governing equations through the multiplication of the vapor Rayleigh number to the nondimensional thermal expansion coefficient and density ratio, and that of vapor Prandtl number to the nondimensional viscosity ratio.

The gravity factor in Eq.(3.8), $\overline{g}$, represents the gravity level. Such expression in the equation leads to an explicit and clear representation for the gravity effect and convenient adjustment for the computation.

In obtaining the above equations, the following dimensionless variables are used

$$\theta = \frac{T}{T_0}, \qquad \overline{\rho}_i = \frac{\rho_i}{\rho_{v,0}}, \qquad \overline{p} = \frac{p}{\rho_{v,0}(\alpha_{v,0} / L)^2}$$

$$X = \frac{x}{L}, \qquad Y = \frac{y}{L}, \qquad = \frac{t}{t_r} = \frac{t}{(L^2 / \alpha_{v,0})}, \tag{3.14}$$

$$U = \frac{u}{(\alpha_{v,0} / L)}, \qquad V = \frac{v}{(\alpha_{v,0} / L)}, \qquad \vec{\overline{V}} = U\vec{e}_x + V\vec{e}_r$$

where $u_r=\alpha_{v,0}/L$ is the thermal diffusion velocity scale in the vapor phase, $\vec{e}_x$ and $\vec{e}_r$ are the axial and radial unit vectors, respectively. Other velocity scales, such as buoyancy velocity scale, *etc.*, can also be used to yield different forms of the governing equations.

The thermophysical properties of UF_4's liquid phase and vapor phase, at a referential state of T_0=2000K and, P_0=1Mpa (10 atm), are given in the Table 2.1 according to Watanabe and

Anghaie (1993) and Anghaie (1992). The initial density ratio of liquid to vapor, $\rho_l/\rho_{v,0}$, is 300, and the initial conductivity ratio, $\kappa_l/\kappa_{v,0}$, is 8.3. The vapor Rayleigh number Ra_v based on the vapor phase properties and the ground gravity level is $1.6\text{x}10^6$, vapor Prandtl number Pr_v is 0.53, and Stefan number St is 0.67. The same amount of thermal power as shown in Section 2.3 and Eq. (3.12) is generated and provide internal heating to the system.

3.3 Numerical Treatment

The fully implicit time marching, with time step size of 10^{-3}, is used for the temporal difference. The hybrid scheme is used for the spatial difference, where the first order upwind scheme for the convection terms and the second order central difference scheme are used accordingly.

The computation is unstable and difficult to converge when only the central difference scheme is used. One reason is that there are the interactions between the natural convection cells in the liquid phase and vapor phase, and the interaction is particularly strong near the liquid-vapor interface, as will be shown later. These interactions make the computation unstable and easily divergent. Another reason is that there is a computational grid limitation of cell Reynolds number, $\text{Re}_{\Delta x}$, or cell Peclet number, $\text{Pe}_{\Delta x}$. When the Rayleigh number or Grashof number is considerably large, a very thin grid has to be adopted, which is time consuming and expensive. As we know, for example, the natural convection velocity scale is $u_r=(Gr_v)^{1/2}\ v/L$, Gr_v is the Grashof number based on vapor properties. Thus the cell Reynolds number, $Re_{\Delta x}=u_r\Delta x/L=(Gr_v)^{1/2}\ \Delta X$. It is required that $Re_{\Delta x}$ be not greater than *2* for the computational stability. To satisfy this, if $Gr_v=10^6$, ΔX must be smaller than *1/500*. Such a dense mesh is not realistic for the computation capacity of

current ordinary work stations. By adopting under-relaxation and more inner-loop iterations for convection equations (see Shyy 1994a), *etc.*, higher $Re_{\Delta x}$, i.e, *10-15*, can be tolerated for some simple problems of natural convection in a single phase system, such as those of cases in chapter 5. Associated with the phase change and the interactions of convection cells between two phases, the computational stability becomes more difficult to be guaranteed. Very dense meshes, *i.e.*, *41x101, 81x201*, were tested for the cases of $\bar{g} = 10^{-3}$, Rav=10^6, and the central difference scheme failed.

Therefore, the first order upwind scheme have to be used for the convection terms to guarantee the computational stability and convergence. The price paid is the lower accuracy of the results. In the following computations, the mesh with 51x101 uniform grids is used. With such mesh and 2000 time steps, the typical CPU time in the Workstation of SunSparc 20 is about 10 ~ 15 days.

3.4 Results and Discussions

The evaporation and condensation processes under micro-gravity and normal gravity conditions, $\bar{g} = 10^{-3}$, and *1*, are modeled. The dependence of the phase change performance on the gravity level is shown clearly. In the following results, the evolution of the liquid-vapor interface topology, the temperature distribution, the flow pattern of natural convection in liquid and vapor phases, are demonstrated.

At the initial state, the liquid and vapor are assumed to be subcooled and superheated, respectively. The dimensionless temperature ranges from 0.8 to 1.0 in the liquid phase and from 1.0 to 1.2 in the vapor phase. The liquid and vapor are saturated at the interface with the initial

saturation temperature of 1.0. The aspect ratio is 2.5. Because of the axial symmetry, only right half of the container with the liquid and vapor is modeled. The internal heat generation provides heat both in the liquid and vapor phases according to Eqs.(2.13), (2.14). At $\tau=0$, the side wall also starts to be cooled with an outward constant heat flux. The concurrent internal heating and external cooling lead to the simultaneous bulk evaporation and condensation. As time marching, more and more heat is generated until t = 420 s ($\tau=1.5$) when the heat generation keeps constant.

3.4.1 At the micro-gravity of 10^{-3} -g

The results of the evaporation/condensation process is shown in Figure 3.1 through Figure 3.5. Using the phase identifier which is the local vapor phase fraction, the distribution of the liquid and vapor phases and the position of the interface are determined. The topology of the liquid-vapor interface and the temperature distribution at various time instants are displayed in Figures 3.1 and 3.2, respectively. The flow fields in the vapor and liquid phases are presented in Figures 3.5(a), (b), respectively.

The internal heat generation evaporates the liquid, while the side wall cooling tends to condense the vapor. Globally, the evaporation of liquid and condensation of vapor take place simultaneously. The local phase-change process, whether evaporation or condensation, is dominated by either the local internal heating or the wall cooling effect, since the internal heat generation is a spatial function. The evaporation is dominant near the central axial position where the heat generation intensity is higher and evaporates more liquid. The condensation caused by the side wall cooling is dominant near the side wall. The simultaneous evaporation and condensation cause the motion and deformation of the interface. Because of the nature of time dependent heat

generation, the local evaporation and condensation, the motion and deformation of interface continue.

As the process evolves, certain amount of liquid is evaporated into vapor due to the internal heat generation which increases at the early time period, as Eqs.(2.13) and (2.14) indicate. Meanwhile, some amount of vapor near the side wall is condensed into liquid due to the cooling of the side wall. At earlier periods, a short piece of liquid film is formed along the side wall owing to the condensation, and the liquid-vapor interface becomes concave because of evaporation. With time increasing, the interface keeps moving and deforming. The liquid film grows longer and thicker, and the position of the interface at the centerline of the container descends lower and lower. When t = 280 s or $\tau = 1.0$, the liquid film grows up to the top end and covers the entire side wall. At t = 448 s or $\tau = 1.6$, the interface at the low central side descends to the lowest point. The liquid phase, which initially fills in the lower part of the container, now forms a long film covering and residing along the entire side wall. After t = 420 s ($\tau = 1.5$), the internal heat generation rate is a constant, as indicated by Eq. (2.14), and the cooling heat flux at the side wall is also kept constant, the system reaches a steady state and the interface no longer moves. The topology of the interface strongly depends on the temperature distribution and the internal heat generation rate distribution which now is independent of time and only a function of space.

The shape of the interface does not follow the heat generation distribution in a form of chopped sine function, as it does in the case of zero gravity. The evolution of the interface topology is different from that of the case of zero gravity where no buoyancy convection is considered. Under the micro-gravity conditions, and due to the weak gravity effect, the buoyancy

induced convection is not strong but it does change the overall characteristics of the phase-change process.

During the transient process, the temperature distribution varies with time. The temperature contours for the entire system become denser and denser, since internal heat generation is increased. After steady state is reached, the axial temperature distribution does not follow exactly the form of chopped sine function, as it does in the case of zero gravity. There is a temperature gradient discontinuity at the interface due to the release or absorption of the latent heat associated with the phase change and the conductivity difference between vapor and liquid. The discontinuity of the temperature gradient can be observed more clearly in the three dimensional temperature distribution displayed in Fig.3.3. There is an obvious fold on the temperature surf where the liquid-vapor interface is precisely located. The temperature gradient in the liquid region is greater than that in the vapor region, since the thermal power density is proportional to the mass density and more heat is generated in the liquid phase. The axial temperature profile on the side wall is much flatter than that in the vapor region. Liquid is a much better conductor than vapor, the liquid film covering the side wall is more isothermalized. This isothermalization effect is expected to satisfy the design feature of the multiphase fuel cell for potential application in space. The formation of the liquid film and its full coverage on the side wall can prevent the side wall from being overheated, which is also the expectation for the application of such multiphase fuel cell. The temperature distribution at each time instant is different from that in the case of zero gravity, since the convection induced by gravity, though very weak in this case, affects the temperature field. The convection are be discussed later.

The transient characteristic of this system can also be seen from the variation of the saturation temperature with the time shown in Fig. 3.4. The saturation temperature decreases a little bit in the early time period when the internal heating is very weak, the side wall cooling effect is dominant. As the internal heating rate increases, the evaporation becomes dominant and the saturation temperature rises. After t = 448 s (τ=*1.5*), as the system gradually reaches the steady state, the evaporation and condensation are balanced and the saturation temperature maintains a constant.

Figures 3.5(a) and (b) display the flow patterns of the natural convection at different time instants in the vapor phase and liquid phase, respectively. Vapor and liquid are two phases with largely different properties, and their flow and heat transfer characteristics are so different that need to be studied separately. In particular, due to the large mass density difference between two phases, the stream functions for vapor and liquid phases are calculated and plotted separately.

During earlier times, several counter-rotating convection cells appear in the liquid phase. It is noticed that the convection in the liquid phase, owing to its higher density, is more intense than that in the vapor phase. The stronger convection cells in the liquid phase may induce convection in the vapor phase. On the other hand, the convection cells in the vapor phase also affect the flow in the liquid phase. These convection cells in both phases interact with each other and affect each other. Globally, the convection strength in both phases increases with time, since the temperature gradients across system become larger and larger gradually.

It is found that the interaction between these convection cells also makes computation more difficult, and the strong under-relaxation and a lot of iterations, i.e., 500 ~ 1000, in each time step have to be used to guarantee the computational stability and convergence.

The global body force, $-g\rho_{i,0}$ in Eq.(3.6) or $-\bar{g}Ra_v \Pr_v \bar{\rho}_{i,0}(\frac{1}{\beta_v T_0})$ in Eq.(3.8), always tends to keep the mass stay or move downward. The liquid phase of larger mass density is subjected to greater body force than the vapor phase. The vapor phase will naturally occupy the space well above the liquid phase in case no bulk condensation involved. In this case, when the condensation occurs along the side wall due to its cooling, some amount of liquid is accumulated at the side wall. The continuing condensation and the accumulation of liquid lead to the formation of a thin and long liquid film along the side wall. Some liquid moves upward and downward, forming the natural convection due to the buoyancy effect caused by the density gradient and temperature gradient across the liquid film. Partial amounts of the liquid in the film is drawn by the body force downward and back to the liquid pool. A reflux cycle is formed by the phase transformation and the mass transfer.

Compared to the results of the zero gravity case, the process of the liquid film formation and development is slower and less amount of liquid is accumulated in the film for the present case of micro-gravity. It is because of the gravitational force and the reflux effect. With the action of the gravity force, the liquid can not move upward as much and freely as it in the 0-g case.

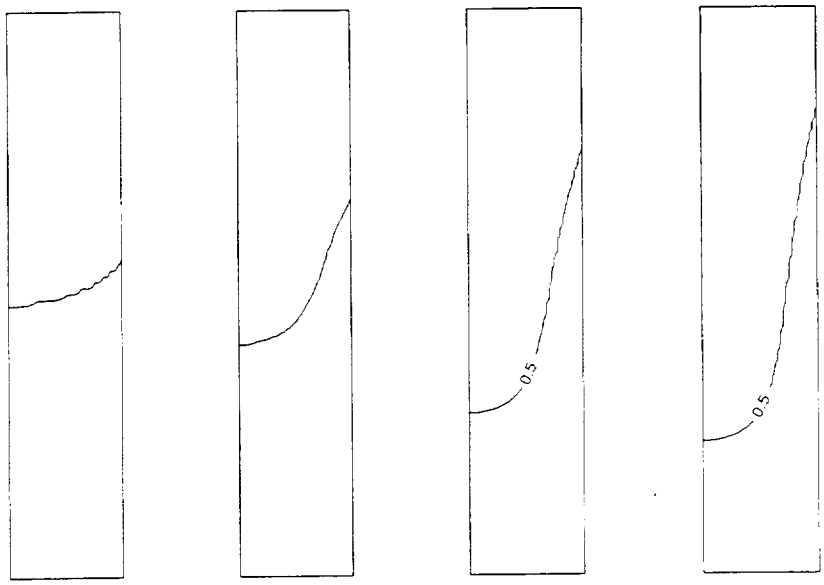

t = 56 (s) 112 (s) 168 (s) 224 (s)
τ = 0.2 0.4 0.6 0.8

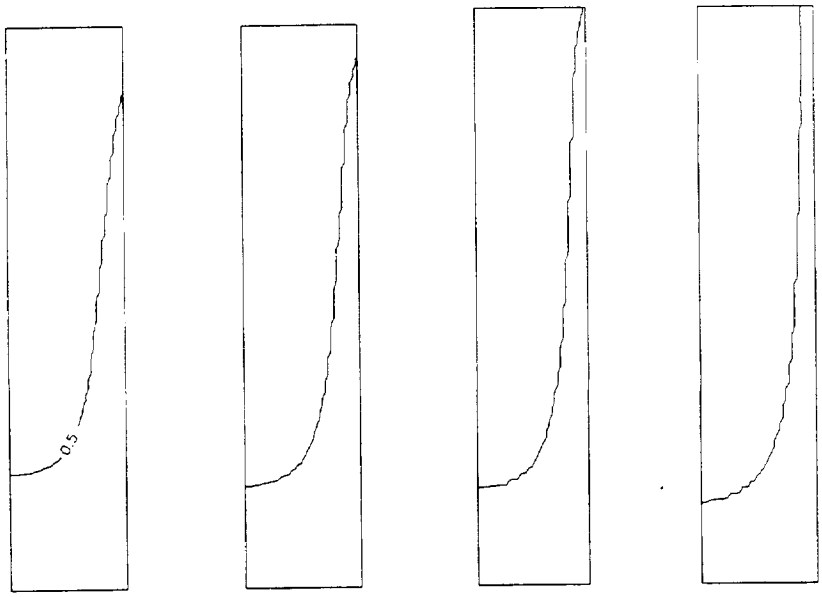

t = 280 (s) 336 (s) 392 (s) 448 (s)
τ = 1.0 1.2 1.4 1.6

Figure 3.1 The evolution of liquid-vapor interface (10^{-3}- g)

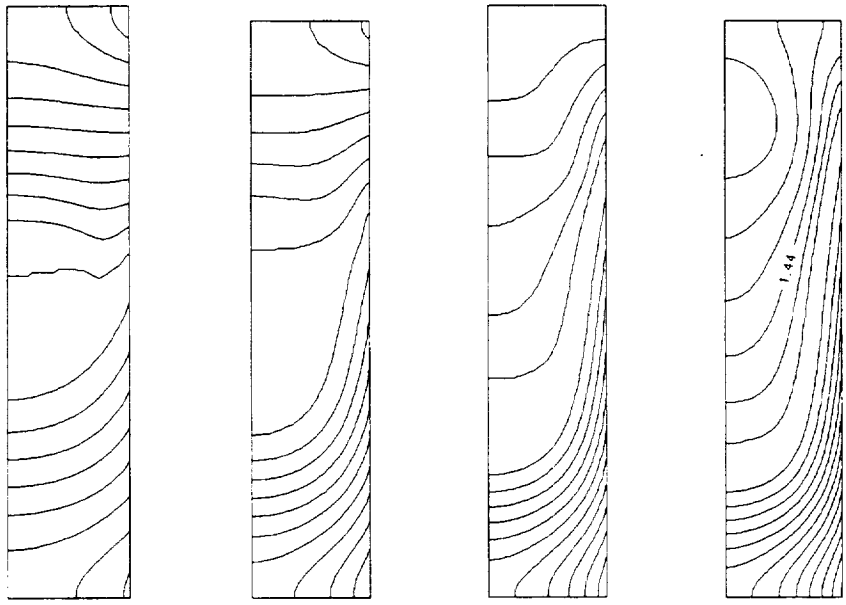

t = 56 (s) 112 (s) 168 (s) 224 (s)
τ = 0.2 0.4 0.6 0.8

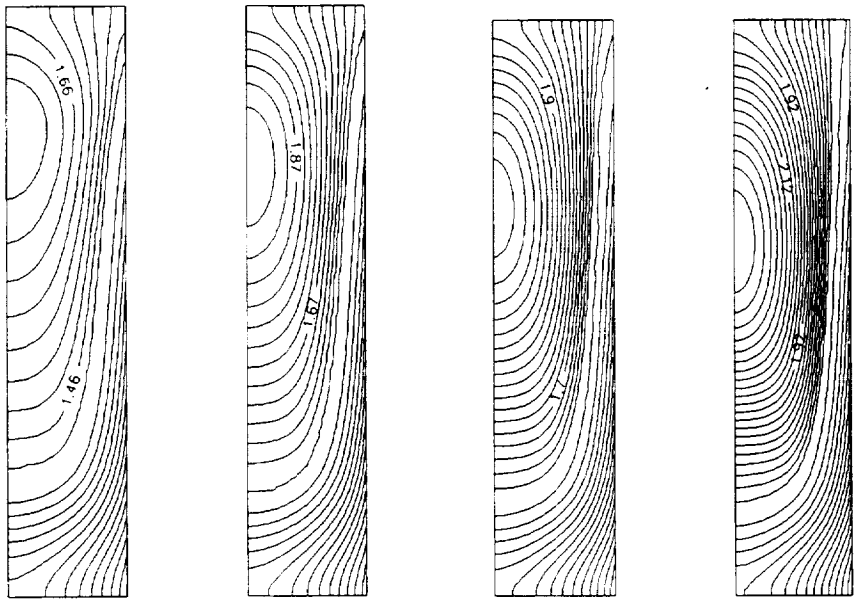

t = 280 (s) 336 (s) 392 (s) 448 (s)
τ = 1.0 1.2 1.4 1.6

Figure 3.2 The evolution of isotherm (10^{-3} -g)

($\Delta\theta = 0.02$, ΔT=40K, the real temperature is $T=\theta x T_0=\theta x 2000K$)

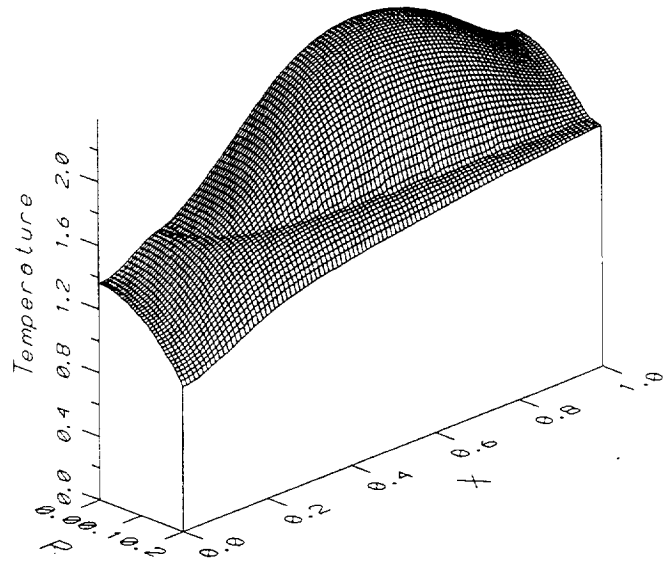

Figure 3.3 Temperature surf and phase distribution at steady state (10^{-3} -g)

(r = RxL = 0 ~ 0.01 m, x=XxL = 0 ~ 0.05 m, the real temperature is $T=\theta x T_0=0 \sim 4000K$)

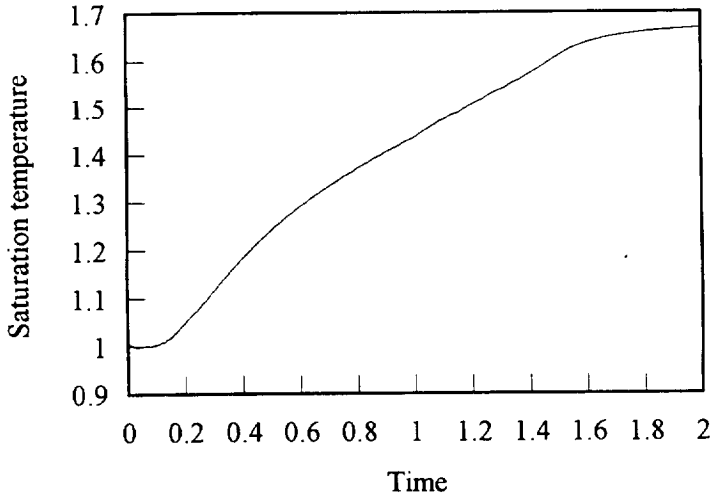

Figure 3.4 Variation of saturation temperature (10^{-3} -g)
(the real time period: 0 ~ 2800 s; the real temperature: $T=\theta x T_0=\theta x 2000K$)

(a) vapor phase

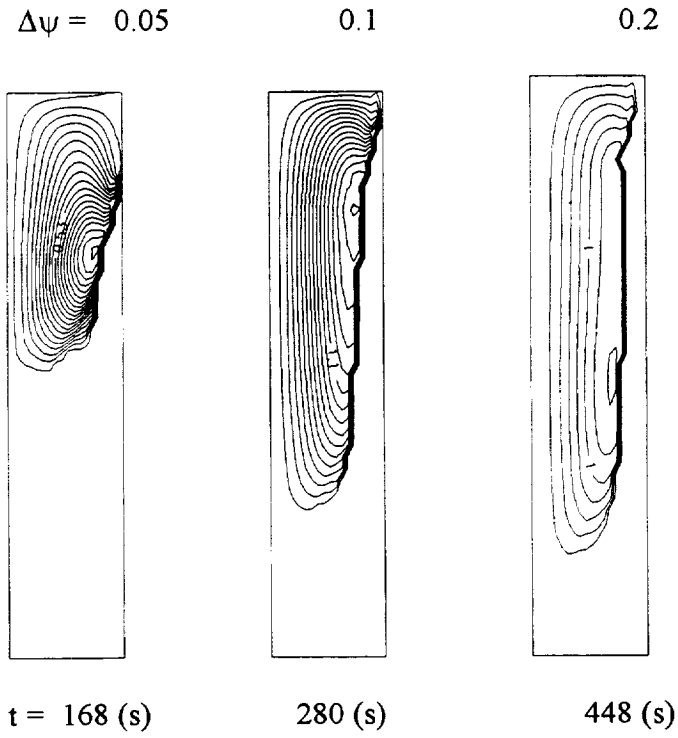

(b) the liquid phase

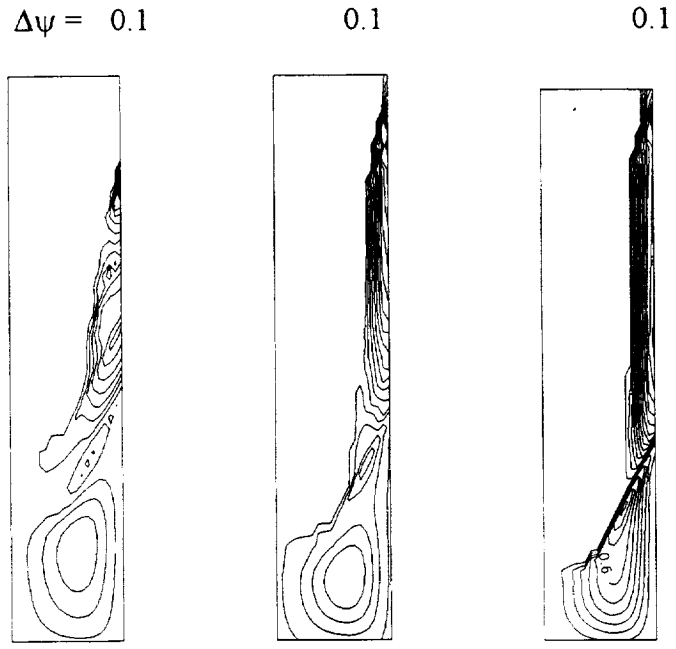

Figure 3.5 Flow patterns in vapor and liquid phases (10^{-3} -g)

3.4.2 At the normal gravity of 1-g

All the boundary and initial conditions are maintained the same as the case of 10^{-3} -g. The gravity factor is 1 in Eq.(3.8). The results are shown in Figure 3.6 through Figure 3.10. The topology of the liquid-vapor interface and the temperature distribution at various time instants are displayed in Figures 3.6 and 3.7, respectively. The flow fields in the vapor and liquid phases are presented in Figure 3.10.

The global evolution of the phase change process is similar to the 10^{-3}-g case. As the time lapses, a piece of thin and long liquid film is formed and more and more liquid is accumulated along the side wall due to the cooling effect. At about t = 336 s (τ =1.2), the liquid film grows up to the top end and covers the entire surface of the side wall. After t =420 s (t=1.5), the system gradually reaches to a steady state when the shape of the liquid-vapor interface, the temperature distribution and the convection flow patterns do not change and evolve with the time.

Significant differences appear in this normal gravity case, compared to the 10^{-3}-g case. First of all, the liquid film grows more slowly than it does with 10^{-3} -g. The liquid film is also thinner. Since the gravity effect is greater in the present case, the liquid film is more readily falling down. More liquid is drawn from the film back to the liquid pool and less liquid is accumulated in the film. And consequently the position of the horizontal surface of the liquid pool is higher than that in 10^{-3}-g case. Secondary, the horizontal surface of the liquid pool becomes wavy, particularly in the position near the end of the liquid film. Such phenomenon does not appear in the case of 10^{-3}-g. The liquid film, though thinner, carries more momentum owing to the greater gravity effect. It impacts the liquid pool and distorts the pool surface.

Furthermore, the temperature distribution is quite different from those at 0-g and 10^{-3}-g. The temperature gradient across the liquid phase is much larger owing to the much intensive internal heat generation rate in the liquid phase. In particular, the temperature gradient across the liquid film is larger than that across the vapor phase, since the liquid film is thinner. Such a thin liquid film with large temperature gradient is a very good conductor for heat transfer. The internally generated heat in the vapor phase, which is less intensive than in the liquid phase, is barely accumulated and easier to be removed outward. Therefore the temperature gradient across the vapor region is nearly zero.

Figure 3.10 shows the flow fields in the vapor and liquid phases. Compared to Figure 3.5, the flow patterns are different. The convection intensity is much larger in 1-g than that in 10^{-3}-g, due to the larger gravity effect. The natural convection cells, in which some a mount of liquid moves upward and downward, are still formed in the thinner liquid film. The reflux of some amount of liquid back to the liquid pool can be seen more clearly.

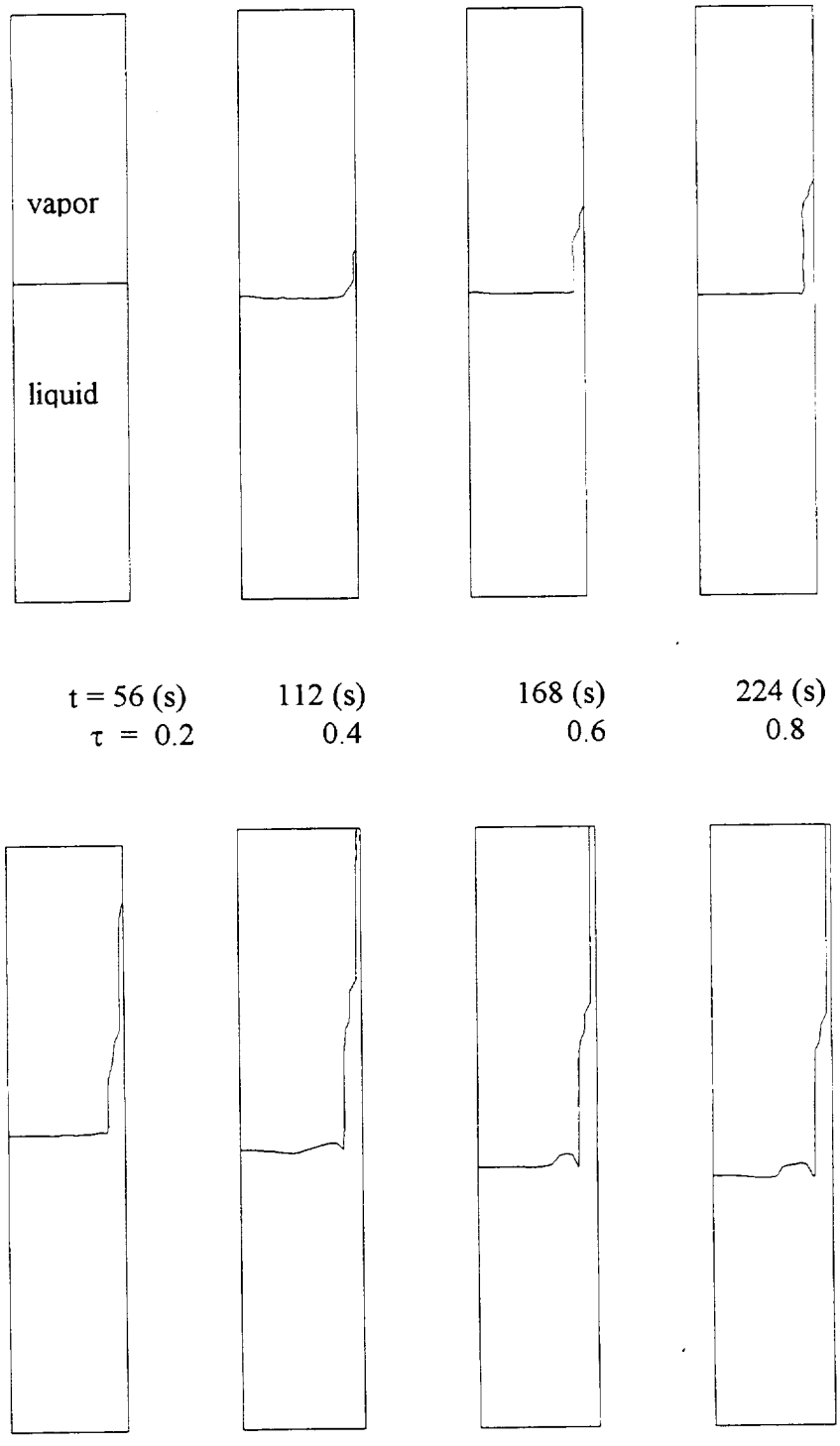

Figure 3.6 The evolution of liquid-vapor interface (1- g)

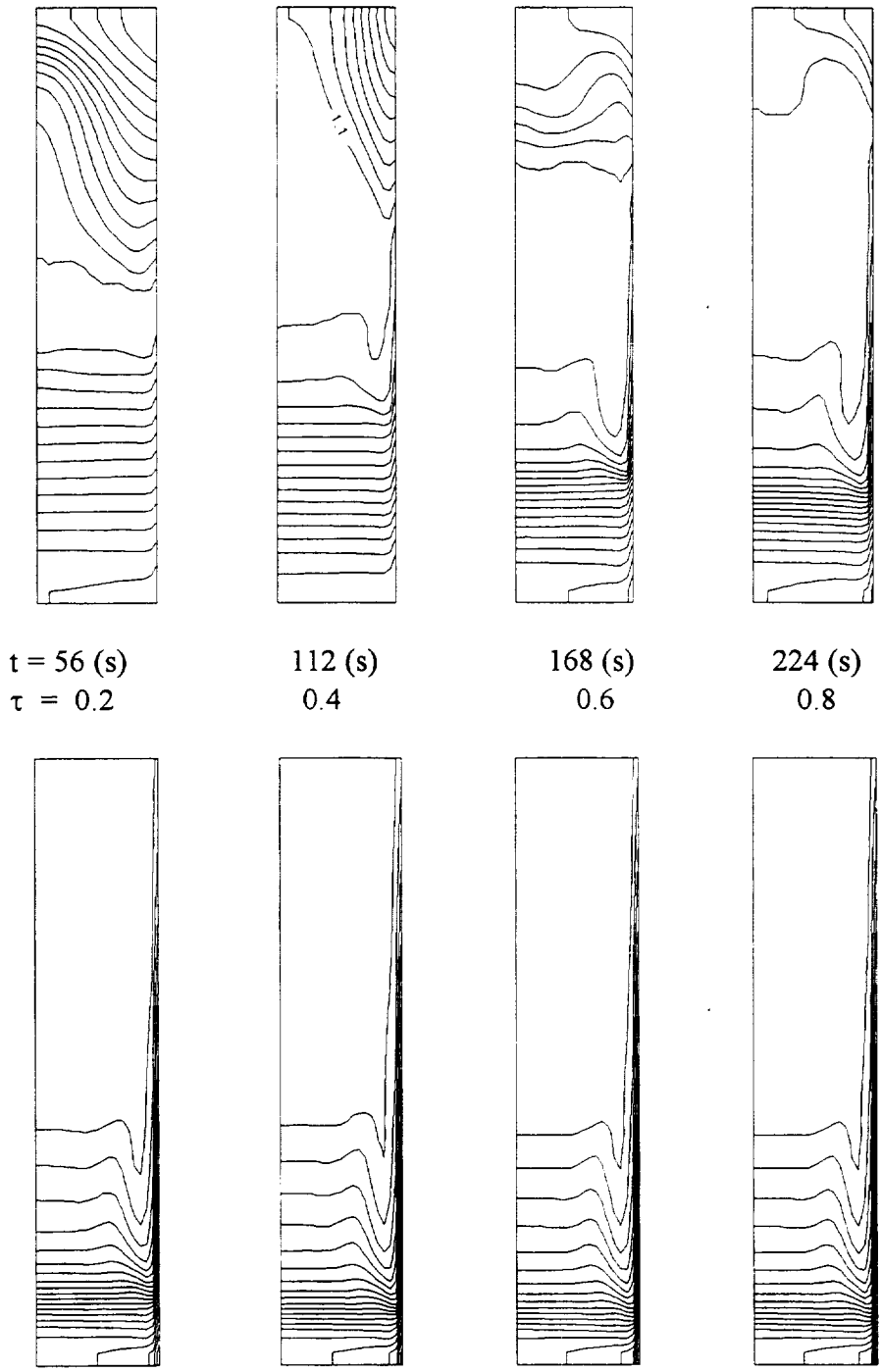

Figure 3.7 The evolution of isotherm (1 -g)

($\Delta\theta = 0.02$, ΔT=40K, the real temperature is $T=\theta x T_0=\theta x 2000K$)

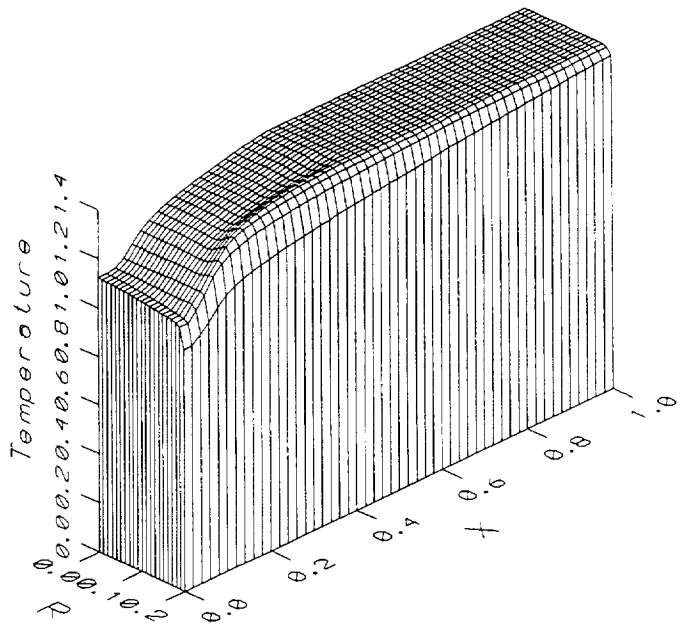

Figure 3.8 Temperature surf at steady state (1 -g)

(r = RxL = 0 ~ 0.01 m, x=XxL = 0 ~ 0.05 m, the real temperature is $T=\theta x T_0=0 \sim 4000K$)

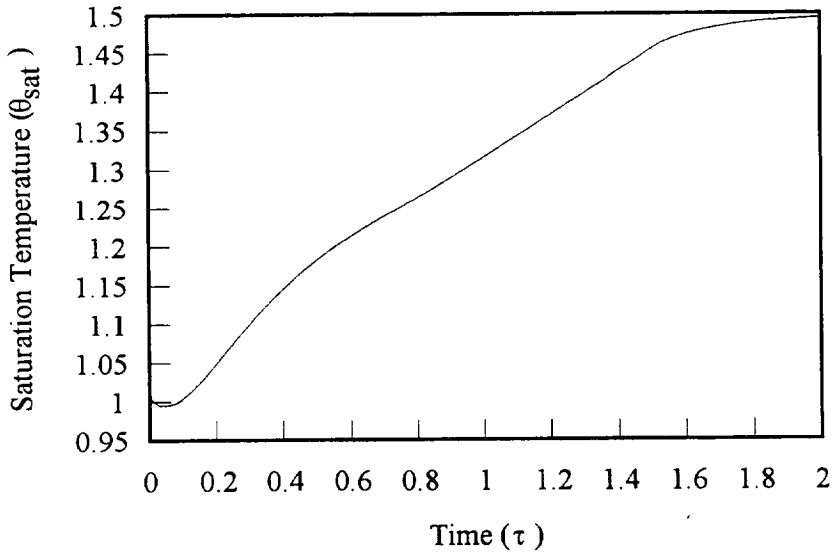

Figure 3.9 Variation of saturation temperature (10^{-3} -g)
(the real time period: 0 ~ 2800 s; the real temperature: $T=\theta x T_0=\theta x 2000K$)

(a) vapor phase

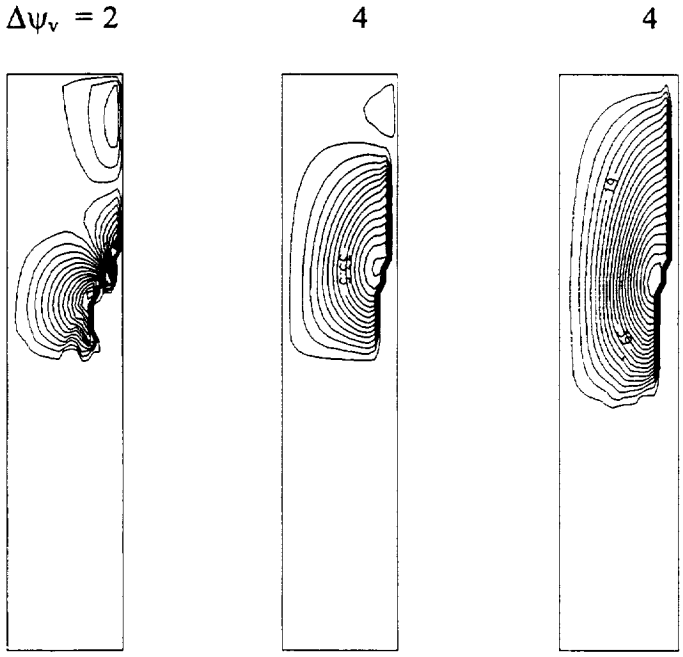

(b) the liquid phase

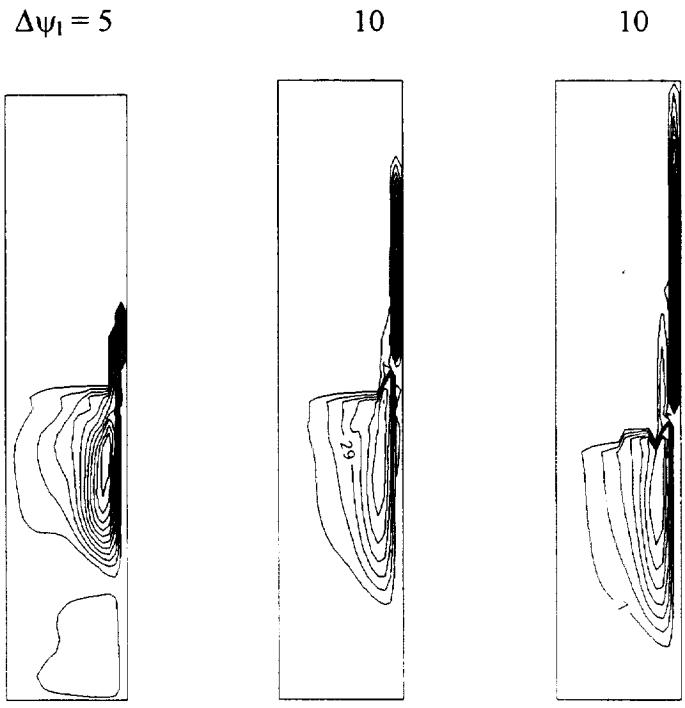

Figure 3.10 Flow patterns in vapor and liquid phases (1 -g)

The differences and the dependence of the phase change performance on the different gravity levels can be observed more clearly in Figure 3.11 where the topology of the liquid-vapor interface, the temperature distribution at the final steady state under three cases, 0-g, 10^{-3}-g and 1-g, are plotted together. The gravity influences on the thermal performance of the bulk liquid-vapor phase change process in the multiphase nuclear fuel cell are displayed explicitly. Under all three gravity conditions, the liquid film is formed and covers the entire side wall, and the liquid film covering the side wall is more isothermalized at the wall surface, which can prevent the side wall from being overheated. At 0-g, the performance is controlled only by the heat transfer, such as internal heat generation and side wall cooling. At non-zero gravity conditions, its performance is controlled by both heat transfer and gravity effects. As gravity increases, the liquid film is thinner, the temperature gradient is larger across the liquid film and is smaller across the vapor phase.

The model developed in this work can be used to provide very useful, and at least qualitative, information for the design and application of multi-phase nuclear fuel elements to be operated under different gravity conditions, particularly when the experiments at micro-gravity environment are expensive and not easy to be conducted.

The current model can also be applied to some two-phase flow problems with or without phase change, for example, the film condensation, the liquid-vapor or liquid-gas flow problems in heat exchangers and material processing equipment.

(a) The topology of the liquid-vapor interface at the steady state

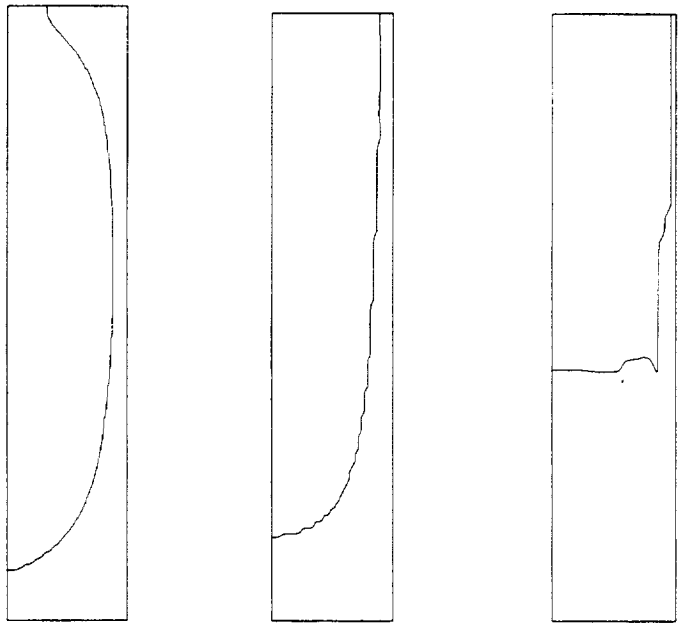

0-g 10^{-3} -g 1-g

(b) The temperature distribution at the steady state

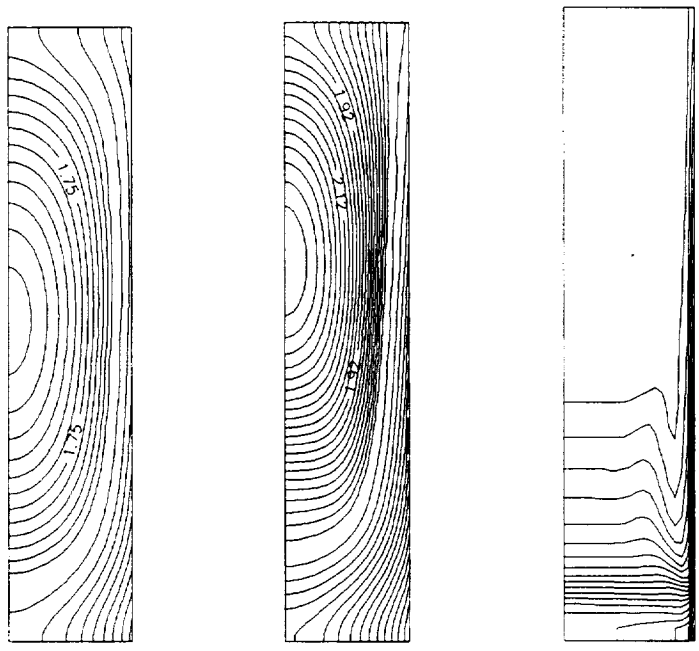

Figure 3.11 Comparison of the interface topology and temperature distribution at different gravity levels

Chapter IV. Conclusions

A unique numerical method has been developed to model the dynamic processes of bulk evaporation and condensation processes, associated with internal heat generation and natural convection under different gravity levels. The internal energy formulation, for the bulk liquid-vapor phase change problems in an encapsulated container, was employed. The equations, governing the conservation of mass, momentum and energy for both phases involved in phase change, were solved.

The thermal performance of a multiphase uranium tetrafluoride fuel element under zero gravity, micro-gravity and normal gravity conditions was investigated. The evolution of the bulk liquid-vapor phase change process, the evolution of the liquid-vapor interface, the formation and development of the liquid film covering the side wall surface, the temperature distribution and the convection flow field in the fuel element were obtained. Numerical modeling results show the strong dependence of the thermal performance of such multiphase nuclear fuel cell on the gravity condition. The differences in the phase change performance of the multiphase fuel element at different gravity levels are quite significant. Under all three gravity conditions, 0-g, 10^{-3}-g and 1-g, the liquid film is formed and covers the entire side wall. The liquid film covering the side wall is more isothermalized at the wall surface, which can prevent the side wall from being overheated. At 0-g, the thermal performance is controlled only by the heat transfer, such as internal heat generation and side wall cooling. At non-zero gravity conditions, its thermal performance is controlled by gravity effect, as well as by heat transfer. As the gravity increases, the liquid film is

thinner, the temperature gradient is larger across the liquid film and smaller across the vapor phase.

This investigation provides valuable, and at least qualitative, information for potential design and application of multi-phase nuclear fuel elements to be operated under different gravity conditions, particularly when the experiments at micro-gravity environment are expensive and not easy to be conducted.

Further effort is worthful and recommended to extend the current model for liquid-vapor phase change problems to a unified triple-phase model. All phase change processes between these three phases, *i.e.*, solid-liquid, liquid-vapor, solid-vapor, or solid-liquid-vapor, can be simulated. This will contribute a lot for the research on materials processing. The current model can also be applied to some two-phase flow problems with or without phase change, for example, the film condensation, the liquid-vapor or liquid-gas flow problems in heat exchangers and material processing equipments.

Acknowledgments

This work was performed for the Department of Defense, Ballistic Missile Defense Organization (formerly SDIO), Innovative Science and Technology Office under contract NAS-26314, managed by NASA Lewis Research Center through INSPI.

This work was supported in part by the University of Florida and the IBM Corp. through their Research Computing Initiative at the Northeastern Regional Data Center.

Helpful discussions with Drs. W. Shyy and J. F. Klausner are greatly appreciated.

References

Acharya, S. and Goldstein, R. J. (1985), Natural convection in an externally heated vertical or inclined square box containing internal energy sources, *J. Heat Transfer*, **107**, 855-866

Anghaie, S. (1990), Internal Document, INSPI, Univ. of Florida, Feb. 1990.

Anghaie, S. (1992), Thermophysical properties of UF4 at high temperatures(1000K<T<10,000K), Internal Report, INSPI, Univ. of Florida

Anghaie, S. and Ding, Z. (1995), Thermal performance of a high temperature phase change thermionic fuel cell, *1995 National heat transfer Conf.*, Portland, Oregon

Bejan, A. (1984), *Convection Heat Transfer*, John Wiley & Sons, New York

Bergman, T. L. and Ramadhyani, S. (1981), Combined buoyancy- and thermocapillary-driven convection in open square cavities, *Numer. Heat Transfer*, **9**, 441-451

Brice, J. C. (1986), *Crystal Growth Processes*, Blackie, London

Brown, R. A. (1988), Theory of transport processes in single crystal growth from the melt, *A.I.Ch.E. Jl*, **34**, 881-911

Buckle, V. and Peric, M. (1992), Numerical simulation of buoyant and thermocapillary convection in a square cavity, *Numerical Heat Transfer*, Part A, **21**, 121-141

Carey, V. P., (1992) *Liquid-Vapor Phase-Change Phenomena*, Hemisphere Pub. Corp.

Carpenter, B. M. and Homsy, G. M. (1989), Combined buoyant-thermocapillary flow in a cavity, *J. Fluid Mech.*, **207**, 121-132

Cossmann, R., Odenthal, H.-P. and Renz, U. (1982), Heat and Mass Transfer During Partial Condensation in a Turbulent Pipe Flow, *Proc. 7th Int. Conf. of Heat Transfer.* U. Grigul et al. ed., Hemisphere Publishing Corp., Washington, D.C.

Crank, J. (1984), *Free and Moving Boundary Problems,* Clarendon Press, Oxford

de Vahl Davis, G. (1983), Natural convection of air in a square cavity: a bench mark numerical solution, *Intl. J. for Numerical Meth. in Fluids*, **3**, 249-264

Ding, Z. (1995), Modeling of bulk evaporation and condensation with internal heating at various gravity conditions, *Ph.D. Dissertation*, Mechanical Engineering Dept., Univ. of Florida

Ding, Z. and Anghaie, S. (1994a), Numerical investigation of the two-phase equilibrium state in a cylindrical nuclear fuel cell under zero gravity condition, *6th AIAA/ASME Joint Thermophysics and Heat Transfer Conf.*, Colorado Springs, CO, AIAA 94-1995

Ding, Z. and Anghaie, S. (1994b), Modeling of R-12 bulk evaporation in an encapsulated container, *ASME Intl. Mechanical Engineering Congress & Exhibition*, Chicago, IL

Ding, Z. and Anghaie, S. (1995a), Numerical modeling of bulk evaporation and condensation with constant volume, to appear in *Intl. J. for Numerical Methods in Engineering*, 1995

Ding, Z. and Anghaie, S. (1995b), Modeling of bulk evaporation, *30th AIAA Thermophysics Conf.*, San Diego, CA

Ding, Z. and Anghaie, S. (1995c), Analysis and formulation of bulk evaporation and condensation problems, submitted to *Intl. J. Heat & Mass Transfer*

Eckter, E. R. G., Goldstein, R. J., et al. (1992), Heat Transfer-a Review of 1991 literature, *Intl. J. Heat and Mass Transfer*, **35**, No.12

Eckter, E. R. G., Goldstein, R. J., et al. (1991), Heat Transfer-a Review of 1990 literature, *Intl. J. Heat and Mass Transfer*, **34**, No.12, 2931-3010

Eckter, E. R. G., Goldstein, R. J., et al. (1990), Heat Transfer-a Review of 1989 literature, *Intl. J. Heat and Mass Transfer*, .**33,** No.12, 2349-2437

Filk, M. I. and Tien, C. L.(1989), An Approximate Analysis for General Film Condensation Transients, *J. Heat Transfer*, **111**, 511-517.

Fusegi, T., Hyun, J. M. and Kuwahara, K. (1992), Natural convection in a differentially heated square cavity with internal heat generation, *Numer. Heat Transfer*, **21**, 215-229

Gau, C. and Viskanta, R. (1986), Melting and Solidification of a pure metal on a vertical wall, *J. Heat Transfer*, **108**, 174-181

Gaultier, M., Lezaun, M. and Vadillo, F.(1993), A Problem of Heat and Mass Transfer: Proof of the Existence Condition by a Finite Difference method, *Intl. J. for numerical Methods in Fluids*, **16**, 87-104.

Gebhart, B., Jaluria, Y., Mahajan, R. L. and Sammakia, B.(1988), *Buoyancy-Induced Flows and Transport*, Hemisphere, Washington D. C.

Gerner, F. M. and Tien, C. L.(1989), Axisymmetric Interfacial Condensation Model, *J. Heat Transfer*, **111**, 503-510.

Hatsopoulos, G. N. and Gyftopoulos, E. P. (1973) *Thermionic Energy Conversion Vol.I: Process and Devices*, MIT Press, Cambridge, MA

Hortmann, M., Peric, M. and Scheuerer, G. (1990), Finite volume multigrid prediction of laminar natural convection: bench-mark solutions, *Intl. J. for Numerical Meth. in Fluids*, **11**, 189-207

Hung, C. I., Shyy, W. and Ouyang, H. (1995), Transient natural convection and conjugate heat transfer in a crystal growth device, *Int. J. Heat Mass Transferm*, **38**, 701-712

Jang, J. H., Faghri, A., Chang, W. S. and Mahefkey, E. T.(1990), Mathematical modeling and analysis of heat pipe start-up from the frozen state, *J. Heat Transfer*, **112**, 586-594

Jones, W. P. and Renz, U. (1974), Condensation from a turbulent stream onto a vertical surface, *Int. J. Heat Mass Transfer*, **17**, 1019-1028

Kimura, S. and Bejan, A. (1983), The "heatline" visulization of convective heat transfer, *J. Heat Transfer*, **105**, 916-919

Lame, G. and Clapeyron, (1831) *Ann. Chem. Phys.*, **47**, 250-256.

Lamp, T. R. and Donovan, B. D. (1992) Thermal Characteristics of Advanced Thermionics Technology Programs at Wright Laboratory, *Proc. 27th Intersociety Energy Conversion Engineering Conference*, San Diego, CA: 21-25

Lee, H., Lewis, B. R. and Klein, A. C. (1993) System Modeling for the Advanced Thermionic Initiative Single Cell Thermionic Space Nuclear Reactor, *Proc. 10th Symposium on Space Nuclear Power and Propulsion*, Conf-930103, M. S. EI-Genk and M. D. Hoover, eds., American Institute of Physics, New York.

Lee, J. and Goldstein, R. J. (1988), An experimental study on natural convection heat transfer in an inclined square enclosure containing internal heat sources, *J. Heat Transfer*, **110**, 345-349

Lewis, B. R., Pawlowski, R. A., Greek, K. J. and Klein, A. C. (1991) Advanced Thermionic Reactor System Design Code, *Proc. 8th Symposium on Space Nuclear Power Systems*, Conf-910116, M. S. EI-Genk and M. D. Hoover, eds., American Institute of Physics,

New York.

McVey, J. B. and Rasor, N. S. (1992) The TECMDL Thermionic Converter Computer Model, *Proc. 27th Intersociety Energy Conversion Engineering Conference*, Society of Automotive Engineers, San Diego, CA: 21-25

Nadarajah, A. and Narayanan, R. (1990), Comparison between morphological and Rayleigh-Marangoni instabilities, Meinkoen, D. and Haken, H. (eds), *Dissipative Structures in Transport Processes and Combustion*, 215-228, Springer-Verlag, New York

Ostrach, S. (1982), Low-gravity fluid flows, *Ann. Rev. Fluid Mech.*, **14**, 313-345

Ostrach, S. (1983), Fluid mechanics in crystal growth-The 1982 freeman scholar lecture, *J. Fluids Engineering*, **105**, 5-20

Ostrach, S. (1988), Natural convection in enclosures, *J. Heat Transfer*, **110**, 1175-1190

Ozisik, M. N. (1980), *Heat Conduction*, John Wiley, New York

Patankar, S. V. (1980), *Numerical Heat Transfer and Fluid Flow*, Hemisphere Pub., New York

Poirier, O. and Salcudean, M. (1988), On numerical methods used in mathematical modeling of phase change in liquid metals, *J. Heat Transfer*, **110**, 562-570

Prakash, C., Samonds, M. and Singhal, A. K. (1987), A fixed grid numerical modeling methodology for phase change problems involving a moving heat source, *Int. J. Heat Mass Transfer*, **30**, 2690-94

Ramaswamy, B. and Jue, T. C. (1992), Analysis of thermocapillary and buoyacy-affected cavity flow using FEM, *Numer. Heat Transfer*, **22**, 379-399

Rasor, N. S. (1991) Thermionic Energy Conversion Plasmas, invited review paper, *IEEE Transactions on Plasma Science*, **19**, No.6

Reynolds, W. C., *Thermodynamic Properties in SI* (1979), Dept. of Mechanical Engineering, Stanford University

Rohsenow, W. M.(1973), "Film Condensation" In *Handbook of Heat Transfer* (Edited by W. M. Rohsenow and J. P. Hartnett), Set. 12A. McGraw-Hill, New York

Samarskii, A. A., Vabishchevich, P. N., Iliev, O. P. and Churbanov, A. G. (1993), Numerical simulation of convection/diffusion phase change problems-A Review, *Int. J. Heat Mass Transfer*, **36**, 4095-4106

Shamsundar, N. and Sparrow, E. M. (1975), Analysis of multidimensional conduction phase change via the enthalpy model, *J. Heat Transfer*, **97**, 333-340

Shyy, W. and Chen, M. (1990), Steady-state natural convection with phase change, *Int. J. Heat Mass Transfer*, **33**, 2545-2563

Shyy, W. and Chen, M. (1991), Interaction of thermocapillary and natural convection flow during solidification: normal and reduced gravity conditions, *J. Crystal Growth*, **108**, 247-261

Shyy, W., Pang, Y., Hunter, G. B., Wei, D. Y. and Chen, M.-H. (1992a), Modeling of turbulent transport and solidification during continuous ingot casting, *Int. J. Heat Mass Transfer*, **35**, 1229-1245

Shyy, W. and Rao, M. (1992b), Convection treatment for high Rayleigh number, laminar, natural convection calculation, *Numerical Heat Transfer*, Part B, **22,** 367-374

Shyy, W., Udaykumar, H. S. and Liang, S.-J. (1993a), An interface tracking method applied to morphological evolution during phase change, *Int. J. Heat Mass Transfer*, **36**, 1833-1844

Shyy, W., Gringrich, W. K., Krotiuk, W. J. and Fredley, J. E. (1993b), Transient two-phase heat transfer in a capillary-pumped-loop reservoir for spacecraft thermal management, *Proc. 10th Symp.m on Space Nuclear Power and Propulsion*, Conf-930103, American Institute of Physics

Shyy, W. and Rao, M. M. (1993c), Simulation of transient natural convection around an enclosed vertical channel, *J. Heat Transfer*, **115**, 946-954

Shyy, W. (1994a), *Computational Modeling for Fluid Flow and Interfacial Transport*, Elsevier, Amsterdam, The Netherlands

Shyy, W. (1994b), Modeling of transient two-phase heat transfer for spacecraft thermal management, *Microgravity Sci. Tech.*, 7, 219-227

Shyy, W. and Rao, M. M. (1994a), Enthalpy based formulations for phase-change problems with application to g-jitters, *Microgravity Sci. Technology*, 7, 41-49

Shyy, W., Liang, S.-J. and Daniel, Y. W. (1994b), Effect of dynamic perturbation and contact condition on edge-defined fiber growth characteristics, *Int. J. Heat Mass Transfer*, **37**, 977-987

Sparrow, E. M. and Eckter, E. R. G. (1961), Effects of Superheated Vapor and noncondensable gases on Laminar Film Condensation, *A.I.Ch.E. Journal*, 7, No.3

Sparrow, E. M. and Lin, S. H. (1964), Condensation Heat Transfer in the Presence of Noncondensable gas, *J. Heat Transfer*, **86**, 430-436

Sparrow, E. M., Minkowycz, W. J. and Saddy, M. (1967), Forced Convection condensation in the Presence of Noncondensables and Interfacial Resistance, *Intl. J. Heat Mass Transfer*, **10**, 1829-1845.

Stefan, J. (1891), *Ann. Phys. Chemie*, **42**, 269-286.

Tournier, J.-M. and El-Genk, M. S. (1992), "HPTAM" Heat-pipe transient analysis model: an analysis of water heat pipes, *Proc. 9th Symp. Space Nuclear Power Systems*, Conf-920104

Yao, L. S. and Prusa, J. (1989), Melting and Freezing, in *Advances in Heat Transfer*, Hartnett et al. ed., Academic Press, Inc., San Diego, **19**, 23-85

Voller, V. R. and Swaminathan, C. R. (1991), General source-based method for solidification phase change, *Numerical Heat Transfer, Part B*, **19**, 175-189

Voller, V. R. and Parakash, C. (1987), A fixed grid numerical modelling methodology for convection-diffusion mushy region phase-change problems, *Int. J. Heat Mass Transfer*, **30**, 1709-1719

Watanabe, Y. and Anghaie, S. (1993) Thermophysical properties of gas phase uranium tetrafluoride, *AIAA 93-2758, AIAA 28th Thermophysics Conf.*, Orlando, FL, July 1993

Yong, T. J., Thayer, K. L. and Ramalingan, M. L. (1993) Performance Simulation of an Advanced Cylindrical Thermionic Fuel Element with a Graphite Reservoir, *AIAA 28th Thermophysics Conference*, AIAA 93-2857, Orlando, FL

REPORT DOCUMENTATION PAGE

Form Approved
OMB No. 0704-0188

1. AGENCY USE ONLY (Leave blank)	2. REPORT DATE	3. REPORT TYPE AND DATES COVERED
	April 1996	Final Contractor Report

4. TITLE AND SUBTITLE

Modeling of Thermal Performance of Multiphase Nuclear Fuel Cell Under Variable Gravity Conditions

5. FUNDING NUMBERS

WU-233-01-0N
C-NAS3-26314

6. AUTHOR(S)

S. Anghaie and Z. Ding

7. PERFORMING ORGANIZATION NAME(S) AND ADDRESS(ES)

University of Florida
Ultrahigh High Temperature Reactor and Energy Conversion Program
Innovative Nuclear Space Power and Propulsion Institute
Gainesville, Florida 32611

8. PERFORMING ORGANIZATION REPORT NUMBER

E-9884

9. SPONSORING/MONITORING AGENCY NAME(S) AND ADDRESS(ES)

National Aeronautics and Space Administration
Lewis Research Center
Cleveland, Ohio 44135-3191

10. SPONSORING/MONITORING AGENCY REPORT NUMBER

NASA CR-198391

11. SUPPLEMENTARY NOTES

Project Manager, Harvey S. Bloomfield, Power Technology Division, NASA Lewis Research Center, organization code 5440, (216) 433-6131.

12a. DISTRIBUTION/AVAILABILITY STATEMENT

Unclassified - Unlimited
Subject Categories 20 and 43

This publication is available from the NASA Center for Aerospace Information, (301) 621-0390.

12b. DISTRIBUTION CODE

13. ABSTRACT *(Maximum 200 words)*

A unique numerical method has been developed to model the dynamic processes of bulk evaporation and condensation processes, associated with internal heat generation and natural convection under different gravity levels. The internal energy formulation, for the bulk liquid-vapor phase change problems in an encapsulated container, was employed. The equations, governing the conservation of mass, momentum and energy for both phases involved in phase change, were solved. The thermal performance of a multiphase uranium tetrafluoride fuel element under zero gravity, micro-gravity and normal gravity conditions has been investigated. The modeling yielded results including the evolution of the bulk liquid-vapor phase change process, the evolution of the liquid-vapor interface, the formation and development of the liquid film covering the side wall surface, the temperature distribution and the convection flow field in the fuel element. The strong dependence of the thermal performance of such multiphase nuclear fuel cell on the gravity condition has been revealed. Under all three gravity conditions, 0-g, 10^{-3}-g and 1-g, the liquid film is formed and covers the entire side wall. The liquid film covering the side wall is more isothermalized at the wall surface, which can prevent the side wall from being overheated. As the gravity increases, the liquid film is thinner, the temperature gradient is larger across the liquid film and smaller across the vapor phase. This investigation provides valuable information about the thermal performance of multi-phase nuclear fuel element for the potential space and ground applications.

14. SUBJECT TERMS

Modeling; Nuclear fuel; Variable gravity; Internal heat generation

15. NUMBER OF PAGES

65

16. PRICE CODE

A04

17. SECURITY CLASSIFICATION OF REPORT	18. SECURITY CLASSIFICATION OF THIS PAGE	19. SECURITY CLASSIFICATION OF ABSTRACT	20. LIMITATION OF ABSTRACT
Unclassified	Unclassified	Unclassified	

National Aeronautics and
Space Administration

Lewis Research Center
21000 Brookpark Rd.
Cleveland, OH 44135-3191